„Dunărea de Jos" University of Galați

Doctoral School of Mechanical and Industrial Engineering

DOCTORAL THESIS

(summary)

Useful information analysis from medical images. Diagnosis improvement by hemodynamic modeling and image processing.

PhD Student,

Cristian-Dragoș OBREJA

Scientific Coordinator,

Prof. PhD. Eng. Phys. Luminița MORARU

Series I4: Industrial Engineering Nr. 51

GALAȚI

2018

„Dunărea de Jos" University of Galați

Doctoral School of Mechanical and Industrial Engineering

Useful information analysis from medical images. Diagnosis improvement by hemodynamic modeling and image processing.

PhD Student,

Cristian-Dragoș OBREJA

Scientific Coordinator,

Prof. PhD. Eng. Phys. Luminița MORARU

Scientific Reviewers

Prof. PhD. Eng. Cristian Vasile DOICIN

Prof. PhD. Eng. Gheorghe OANCEA

Prof. PhD. Eng. Phys. Habil. Antoaneta ENE

Series I4: Industrial Engineering Nr. 51

GALAȚI

2018

Seriile tezelor de doctorat susținute public în UDJG începând cu 1 octombrie 2013 sunt:

Domeniul **ȘTIINȚE INGINEREȘTI**

- Seria I 1: **Biotehnologii**
- Seria I 2: **Calculatoare și tehnologia informației**
- Seria I 3: **Inginerie electrică**
- Seria I 4: **Inginerie industrială**
- Seria I 5: **Ingineria materialelor**
- Seria I 6: **Inginerie mecanică**
- Seria I 7: **Ingineria produselor alimentare**
- Seria I 8: **Ingineria sistemelor**

Domeniul **ȘTIINȚE ECONOMICE**

- Seria E 1: **Economie**
- Seria E 2: **Management**

Domeniul **ȘTIINȚE UMANISTE**

- Seria U 1: **Filologie- Engleză**
- Seria U 2: **Filologie-Română**
- Seria U 3: **Istorie**

ACKNOWLEDGMENTS

At the end of the doctoral program, I feel honored to address words of sincere gratitude **Prof. PhD. Eng. Phys. Luminiţa Moraru**, for the support, trust, patience and encouragement given in the difficult moments that emerged during the elaboration of the doctoral thesis.The suggestions she gave me and the frequent discussions led to the continuous improvement of the thesis.

I would like to thank **Prof. PhD. Phys. Mirela Praisler**, for the support and the constructive suggestions given in the development of this thesis and during the research activity.

I would also like to express my gratitude to **Prof. PhD. Eng. Phys. Habil. Antoaneta Ene** for collaboration, trust and help in developing hemodynamic modeling methods on the retinal circulatory system.

I would also like to thank for the collaboration and support to **Assoc. Prof. PhD. Emil Dănilă.**

Also, I would like to thank the entire staff of the Department of Chemistry, Physics and Environment of the Faculty of Science and Environment, at the "Dunarea de Jos" University in Galati, for the support and for the scientific and friendly environment created.

I would also want to thank my colleague **PhD Simona Moldovanu** for the collaboration and support, regarding the processing, investigation and diagnosis of information in digital images.

Last but not least, I would like to thank my family for their patience, understanding and moral support throughout the PhD thesis preparation.

Galați, March 2018

Eng. Cristian-Dragoș Obreja

Table of contents

KEYWORDS:

Dempster-Shafer fusion, haemodynamic modeling, diabetic retinopathy, retinal vascular system, ESSIM, clustering, segmentation, edge detection

Introduction

The largest amount of information received by a person is through images. They are made using the visual system by projecting information onto the retina and transmission to the optical center of the brain for interpretation. The main problem of the human acquisition and interpretation system for images is the fact that people are unable to retain the details in the images, which usually contain a wide range of useful information.

This natural barrier of the human brain has been overcome by the emergence and continued improvement in image acquisition technologies and storage methods. Due to these developments, it is possible to analyze and interpret acoustic images, those obtained by ultrasound or magnetic field gradients and other images invisible for the human visual system, but commonly used in industrial, aerospace or medical applications.

Due to the advances made in recent decades, image processing has penetrated all branches of modern science. These includes areas such as satellite imaging, robotics, industrial engineering, virtual reality, medical imaging or multimedia databases.

In order to achieve the expected results of the research covered by this thesis, the following image processing stages have been completed:

- Acquisition of digital images, which is accomplished with video cameras, optical microscopes, scanners and medical imaging instruments that digitize the received signal and generate an image.
- Pre-processing, which is a set of techniques aimed at improving complex images in terms of visual appearance and reduction of noise and artifacts generated by the acquisition devices, manipulating brightness and contrast, or emphasizing edges.
- The image texture analysis that is often used in industrial applications and medical imaging and uses generally two types of textures to extract information from digital images.
- In the segmentation stage, a digital image is decomposed into its components. This process extracts from the image either objects and/or regions of interest that satisfy certain uniformity criteria. Segmentation is based either on the properties of discontinuity aimed at edges detection or on the properties of similarity between objects or compact regions.

- The last step is the description, recognition, classification and selection of the of the objects properties in the image. These operations are evaluated using advanced statistical techniques and quality metrics.

Following this steps, we have made theoretical and practical contributions to the processing and evaluation of digital retinal images, thus developing original processing techniques.

Motivation

In many areas, the analysis of digital images obtained through different technologies has become a subject of major importance. The main reason for choosing this research theme is the multidisciplinary character of the research, namely the possibility to apply knowledge specific to physics (flow of fluids), mathematics (statistics) and computer science (software use) in medicine. The paper focuses on the interpretation of retinal images, starting from World Health Organization and International Diabetes Federation statistics, which finds that diabetes is the most prevalent disease at European level and causes one of the highest rates of morbidity and precocious mortality. This interdisciplinary connection offers the possibility of modeling, analyzing and extracting information specific to the general, cerebral and retinal vascular system and determining the presence of specific diseases

In the last decades, image acquisition technology has evolved and is closely related to the advancement of digital image processing technologies. Today's acquisition technologies have the disadvantage that they can only process a certain type of image, and their quality can be affected by noise, brightness or various external factors. To minimize or even eliminate these disadvantages and to improve image quality, we have used a wide range of pre-processing methods. Pre-processing was performed using filters derived from Gaussian functions, rotated at different angles. The main goal pursued was to eliminate noise and improve contrast. Another method of image enhancement was based on image division in regions with different structural features. The goal is to eliminate the uneven illumination in the image that affects the detection of various anomalies.

The images used in this study come from the medical field, because they allow for more in-depth analysis due to their complexity. We have used images of the human vascular system, and the developed methods can easily be transferred to other branches of science or industry.

Research importance

Currently, imaging is present in all branches of science, and the acquisition of images that are not disturbed by external factors arouses interest in scientific research. Digital images unaffected by disturbing elements, such as noise, contrast and uneven illumination, allow a correct understanding of its contents.

For processing digital images and obtaining experimental results we used the following software tools: Matlab 2014a with the following packages and libraries, Graphical User

Interface, Image Processing Toolbox, Wavelets; image analysis and processing software ImageJ (National Institutes of Health, Bethesda, Maryland), and software for statistical analysis SPSS 17.0 (SPSS Inc., Chicago, Illinois).

Following the research of the specialized literature and the implemented applications, it was generated an extra knowledge to the processing and information extraction methods from the medical images of the circulatory system.

Thesis objectives

The research objectives consist in modeling, processing and extraction of useful information from digital images of the retinal vascular system using image segmentation and fusion methods. These techniques generate images of superior quality to original ones.

According to the research themes approached in the scientific papers and the title of the thesis "Useful information analysis from medical images. Diagnosis improvement by hemodynamic modeling and image processing" have been proposed and achieved the following objectives:

- Hemodynamics of blood flow in blood vessels specific to retinal vasculature and determining of blood pressure and blood flow using the physics principle of mass preservation and the principle of minimal energy that allows parametrization of the diameter and the blood flow between the parental branches and the daughter branches of the vascular tree.
- Improving image quality by selectively removing disruptive information such as noise, and eliminating other artifacts generated by the acquisition device using linear and nonlinear filters and Fourier transform.
- Highlight areas of interest by adjusting illumination and contrast, and accentuating edges.
- Detecting blood vessels from complex digital images by segmenting them using edge detection methods and then measuring diameters.
- Improving edge detection capability by using image fusion method based on the Dempster-Shafer algorithm.
- Using methods of segmentation evaluation by statistical and similarity methods.
- Evaluating the performance of edge detection methods using operators (Pratt's Figure of Merit and edge-based structural similarity) that analyze the structural similarity of images.

Thesis structure

The PhD thesis titled "Useful information analysis from medical images. Diagnosis improvement by hemodynamic modeling and image processing" is organized into five chapters, to which we added the introduction and final conclusions.

The **introduction** presents a brief description of the field of digital imaging and the stages of the research. Also in this part are presented the importance and motivation of the chosen theme.

Chapter 1 describes the types, properties and constitutive elements of digital images.

Chapter 2 presents the basics of fluid flow modeling with emphasis on blood vessels hemodynamics. Topical methods are presented, with useful results from existing scientific papers. The subchapter of personal contributions presents the methods used and tested during the research period, including Poiseuille's law and Kirchhoff's laws, and the results achieved.

Chapter 3 is centered on describing methods for classifying digital image characteristics using classification algorithms and statistical evaluation techniques. Investigational methods are predictive (k-nearest neighbors) and descriptive classification, computing of distance-type metrics, Bayesian theory, and k-mean clustering algorithm.

Chapter 4 introduces advanced segmentation methods for extracting objects of interest in the image, that are grouped into histogram, regions and active contours based methods. Analysis of segmentation efficiency is achieved by image fusion techniques. The chapter is completed by personal contributions made to improve segmentation of digital images.

Chapter 5 presents methods for analyzing the quality and precision of image processing techniques, using methods to verify the structural similarity of images and advanced statistical evaluation techniques.

Chapter 6 presents the general conclusions of the paper and the future research directions.

Research results dissemination

The dissemination of the results of the research carried out during the doctoral stage was made by publishing 10 scientific papers in the scientific journals and volumes of the international and national conferences and 8 papers presented at international and national conferences. Of these, a paper is published in the ISI Web of Science Index, a book chapter was published in the Elsevier Health Books collection, three papers are indexed to ISI Proceedings and five papers are published in BDI indexed journals.

Chapter I

Types and properties of digital images

1.1 The mathematical model of the image

The images represent two-dimensional signals that reflect the gray level in the point of coordinates x and y. A two-dimensional image can be expressed as a continuous or discreet pattern. [1]

1.1.1 The continuous pattern of the image

A set of values, placed in a space of two or more dimensions, represents a digital image. From a mathematical point of view, images can be in gray and in color. The color image (RGB) is represented as follows: for each pair of coordinates, a color is assigned (red R, green G, blue B). [2,3]

Figure 1.1 Grayscale image representation

1.1.2 The discreet pattern of the image

Temporal discretization is called sampling and discretization in amplitude is called quantization. By sampling and quantization the transition from continuous to the discrete domain is realised [4].

- Sampling is defined as retriving the intensity and color information from the image in points on a sampling grid.
- Quantisation is a process of transforming the values of a function *f(x,y)* into discrete values [1,4].

1.2 Digital images types

Digital images are a multitude of encoded numerical values of two-dimensional images. Digital images are made up of image elements called pixels. The types of images used in this study are:

- RGB images, where each pixel is represented by three values in RGB space.
- Binary images are represented by a logical array where each pixel is represented on one bit.
- In the intensity images the pixel values are the result of the illumination intensity.
- In the indexed images the value of each pixel is an index which encodes the color of that pixel [3].

1.3 Digital image properties

Digital images are generally acquired using an image sensor and have the following properties: the pixels are arranged in the form of a rectangular network, the image is composed of finite size elements and the image is a 2D array in which the elements are integer numbers, with values between 0 and 255. Digital images have two types of properties: metric or topological.

1.3.1 Metric properties of digital images

The distance between two pixels in a digital image is a quantitative dimension. The distance between the coordinate points (i,j) and (k,l) is defined as it follows:

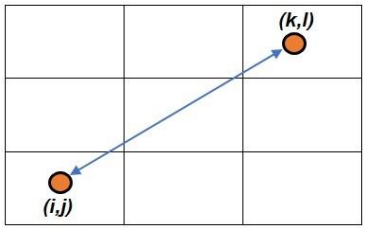

Figure 1.2 Representation of the Euclidean distance

- Euclidean distance. The advantage of this way of distance definition is that it is intuitive and the main disadvantage is the presence of a high computational cost;
- Manhattan distance is used when only horizontal and vertical movements are allowed;

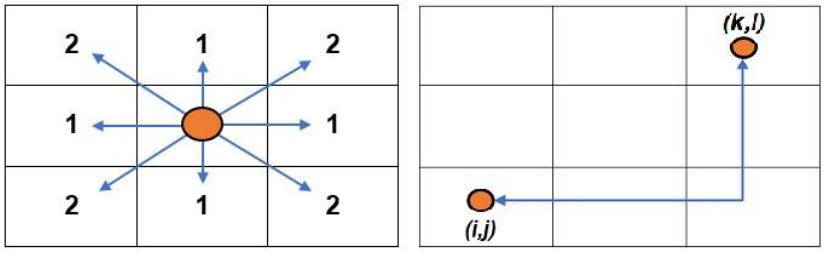

Figure 1.3 Representation of the Manhattan distance

- In RGB space, the distance is given by the distance between two colors c_1 and c_2: $d(c_1,c_2)=\sqrt{d_x^2+d_y^2+d_z^2}$, where d_x, d_y and d_z are the distances on the three axes Ox, Oy and Oz [5,6].

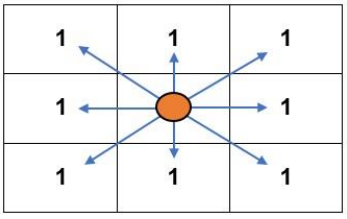

Figure 1.4 Representation of the chess distance

- Chebychev distance (chess distance). This distance is used if, in addition to horizontal and vertical movements, diagonal movements are allowed also [5].

1.3.2 Topological properties of digital images

In image processing, pixel distribution is an important notion. The relationships between pixels that make up 2D images are based on two types of neighborhoods: the first type is composed only from horizontal and vertical neighbors, while the second includes the diagonal ones [7]. Based on the pixel neighborhood, regions can be defined as sets of connected pixels.

A region is a set of pixels in which there is a connection between any pair [5]. An object is joint when there is a path from a selected pixel to any other pixel, passing through adjacent pixels.

Two types of border exist, internal and external. The internal boundary of a region is represented by the set of pixels in the region that have at least one neighbor outside the region. The external border is the edge of the region. The human visual system uses the edge as the first element in recognizing objects or specific features in an image [4,5].

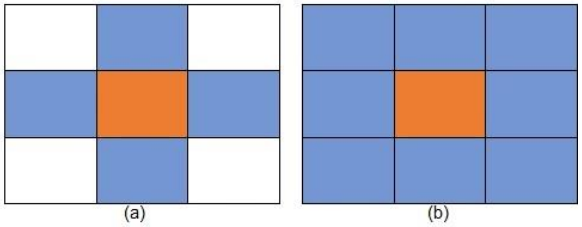

Figure 1.5 Types of pixel neighbors. (a) horizontal and vertical neighbors; (b) horizontal, vertical and diagonal neighbors.

The edge, as a basic element in the characterization of an image, is defined as the property of a pixel and the area in its immediate proximity. It is described by one amplitude and one direction and is a local property of the gray level variation function of an image. The direction of an edge is perpendicular to the gradient direction. There is a connection between edges and borders [8].

Chapter II

Hemodynamic modeling and simulated vascular geometry

The geometry of the vessel influences blood flow pattern and has a decisive influence on health and disease. It is very difficult to predict and to obtain results on pressure and flow at any site in the vascular system. Branched networks, including those of mammals, have been extensively studied in terms of transport properties, structure and function, symmetry or asymmetry [9,10].

2.1 Simulated vascular geometry

The proposed model takes into consideration, in the simulations, both arterial and venous flows. The flow proceeds from a single inlet arteriole vessel, passes through many small vessels and the outlet terminal is a venule. The arterial diameter, decreases progressively to periphery. The geometry of the simulated vascular tree is presented in figure 1.There are four generations of vessel (parent and daughter vessels) with ten bifurcations (denote by Ni). Red indicates the arterioles and letters in square denote the venules. E1 and E15 indicate the inlet and outlet branches. The area of the cross sections is specified to vary according to asymmetry parameter value (δ) and branching attributes. The blood volume of the parent vessel $V_{(p;i;j)}$ is partitioned between its daughters as $\delta V_{(p;i+1;2j)}$ and $(1-\delta)V_{(p;i+1;2j+1)}$.

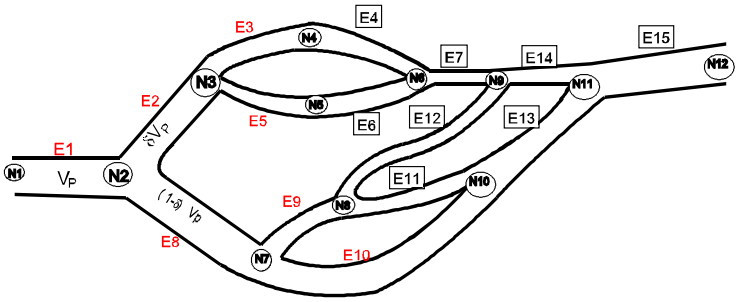

Figure 2.1 The geometry of the simulated vascular tree.

2.2 Structure and flow of fluids in the vascular tree

2.2.1 Mechanical characteristics of blood vessels

Darcy's law characterizes the relationship between blood flow (Q), pressure gradient (ΔP) and resistance encountered by the fluid on a vascular segment (R) [11].

***Blood* flow** is the volume of fluid that crosses a section of a blood vessel over a period of time [11].

Vascular conduction represents the blood flow that passes a blood vessel and has a pressure gradient of 1 mm Hg / m between its ends [11].

The **kinematic and dynamic viscosity** represents an internal force of the fluid, generated by the friction between the blood components.

2.2.2 Navier-Stokes equations

The blood flow in the circulatory system is described based on the Navier–Stokes equations. This equations are based on the the second law of dynamics and the property that the fluid tension is proportional with the variation of speed, viscosity and pressure [12].

2.2.3 Vascular resistance. Poiseuille's law

Vascular resistance is the opposition that blood encounters when advancing through the vascular tree. If both, the fluid and the system are considered ideal cases, the vascular resistance is calculated using the equation:

$$\frac{Q}{\Delta P} = \left(\frac{r^4}{l}\right) x \left(\frac{l}{\eta}\right) x \left(\frac{\pi}{8}\right) \tag{2.1}$$

where Q represents the blood flow, ΔP the difference between the pressure at the start and end of the tube, r represents the radius of the tube, l is the length and η is the viscosity of the blood. The flow rate Q is proportional to the pressure drop across the tube length and the fourth power of the tube radius.

2.2.4 Murray's law

In an attempt to simplify the analysis of a very complex vascular tree structure and to predict the diameters of branching vessels in the cardiovascular system, Murray [13] derived an equation based on the principle of minimum energy.

2.2.5 Kirchhoff's laws

According to Kirchoff's law, for a system with one entry and one exit, the sum of the incoming and outgoing fluid flows is zero. Specifically, the quantity of fluid entering the system is always the same as the output [14].

2.3 Personal contributions

2.3.1 Blood pressure and flow values in small vessels angioarchitectures: application for diabetic retinopathy

The proposed model takes into consideration both the arterial and venous flows. The flow proceeds from a single inlet arteriole vessel, passes through many small vessels and the outlet terminal is a venule. The measured asymmetry parameter has the value 0.4, computed according to Murray's law. The inertia effect of flow has been neglected. Also, we neglected the precise geometric form of the bifurcations and junctions. In order to compute the flow, the total resistance of the structure is estimated. The blood viscosity is assumed to be constant.

The DRIVE retinal image database has been used to test the developed approach. The experiments were conducted on clinical images of normal human eye and afectted by diabetic retinopathy. [15]

In this section we present the pressure gradient and flow rate profiles between nodes. All measurements were based on the same set of parameters. Blood was considered as an

incompressible Newtonian fluid with blood density $\rho = 1060\,Kg/m^3$ and blood viscosity $\mu = 3.5 \cdot 10^{-3}\ Pa \cdot s$.

The outlet pressure is the known parameter of the system and had the same values for all experiments. An unpaired t test and a level of significance p<0.001 were used to assess differences between NHR and DR.

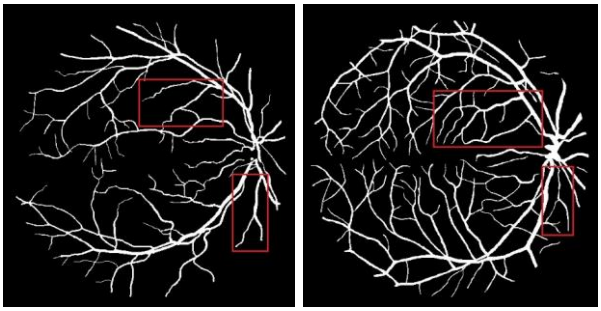

Figure 2.2 Examples of hand-segmented and binarized image from the DRIVE database. a) Normal human retina (NHR); b) diabetic retinopathy (DR).

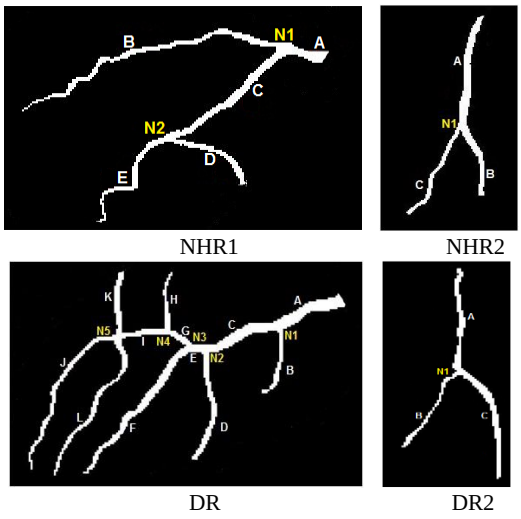

NHR1 NHR2

DR DR2

Figure 2.3 Selected vascular architecture of a normal human retina (NHR) and diabetic

Figure 2.3 presents examples of the cropped areas from retinal images. Depending on the vascular architecture, a variable number of points were defined to establish the blood pressure and flow. Tables 2.1 and 2.2 show the parameters of the regions of interest of vascular trees, for each branch and δ = 0,4. The retinal vessels have the diameter range 250–650 μm and length range 1400–14000 μm. According to the data in tables 2.1 and 2.2, changes to the blood vessels exist.

Table 2.1 The parameters of the region of interest of vascular trees for each branch and for asymmetry parameter δ = 0.4 for two normal human retina ROIs

Vessel segment	Diameter [μm]	Length [μm]	Vessel segment	Diameter [μm]	Length [μm]
NHR1			NHR2		
A	577	2106	A	604	8152
B	331	13660	B	509	4242
C	447	7131	C	350	7749
D	262	4282	R_{eff}[kg mm^{-4} s^{-1}]		0.629
E	345	4457	Inlet pressure [Pa] (mm Hg)		3764
R_{eff}[kg mm^{-4} s^{-1}]		0.499			
Inlet pressure [Pa] (mm Hg)		3797 (28.5)			

Table 2.2 The parameters of the region of interest of vascular trees for each branch and for asymmetry parameter δ = 0.4 for two diabetic retinopathy ROIs

Vessel segment	Diameter [μm]	Length [μm]	Vessel segment	Diameter [μm]	Length [μm]
	DR1			DR2	
A	610	4012	A	327	5859
B	257	3901	B	241	4243
C	557	4160	C	370	6917
D	274	6251	R_{eff}[kg mm^{-4} s^{-1}]		0.310
E	407	1046	Inlet pressure [Pa] (mm Hg)		3116 (23.4)
F	408	7918			
G	284	1432			
H	246	3063			
I	315	2583			
J	306	9100			
K	346	2164			
L	318	8806			
R_{eff}[kg mm^{-4} s^{-1}]		0.326			
Inlet pressure [Pa] (mm Hg)		3176 (23.9)			

The main contribution of this study is the quantification of the blood pressure gradients and the blood flow heterogeneity related to the vascular architecture and branching asymmetry of retinal vascular trees. We observed a decrease in both retinal blood flow and pressure for patients with DR. In the DR, abnormal new blood vessels (neovascularisation) are formed at the back of the eye. They can burst and bleed and blur the vision because these new blood vessels are fragile. For all the analyzed images the vessel diameters are smaller in DR than in

NHR. Similarly, blood pressure as well as flow values tended to be decreased in patients with DR and clear differences in the blood flow profiles exist between NHR and DR images. Pressure and flow patterns were calculated and compared in all bifurcation sites.

Our data is in agreement with previous studies, indicating decreased retinal blood pressure and flow in diabetic retinopathy. Compared with these previous studies our method provides local information about the measured quantities, i.e. at each node of vessel tree. However, this wide range of experimental results clearly indicates that this topic remains very challenging. It has to be noted that individual blood flow analysis is subject to the limitations of time and facilities because the most demanding step is the effective computation of the R_{eff}. Thus, the proposed model contains the following limitations: (i) it does not take into account the local geometry at the vessel bifurcations; (ii) it does not incorporate the elastic properties of the arteriole walls; (iii) the geometry of the eye could affect the experimental determination of the pressure and flow values, and (iv) the wall friction in the vessel was neglected.

2.3.2 Characterization of vascular tree: responses of blood pressure and flow to branching patterns with various geometries

Within an organ, the vessels are arranged in-series and in-parallel. A small artery is in-series with its two daughter branches, and each of these arteriolar branches is in-parallel to each other. Overall, the vascular system is a circuit connected in-series that keeps blood flow equal to that of cardiac output.

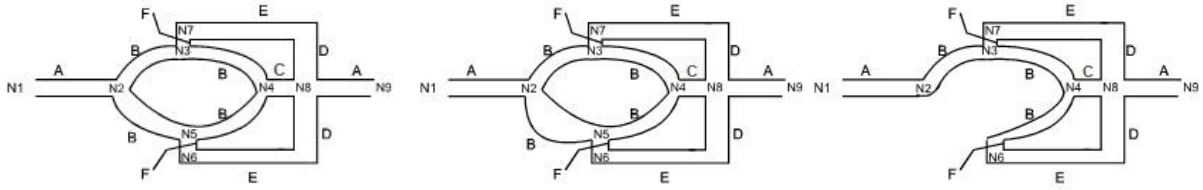

(a) *(b)* *(c)*

Figure 2.4 The geometry of the simulated vascular tree. a) normal vascular tree; b) aneurysm in the branch B, between the nodes N2 and N5; c) stenosis when the branch B has the vascular resistance very high due to the vessel obstruction. There are two generations of vessel (parent and daughter vessels) with seven bifurcations (denote by N). The area of the cross sections are specified to vary according branching attributes (parent or daughter)

The geometry of the simulated normal vascular tree, aneurysm and stenosis are presented in figure 2.4. The proposed vascular system contains a number of small vessels designed in-series and in-parallel along a given length. The precise geometric form of the bifurcations and junctions has been neglected. In order to compute the flow, the total resistance of the structure is estimated. These values show how blood flow and pressure are distributed in each node of the vascular tree.

Table 2.3 Distribution of blood pressure and flow at each node of the vessel tree (for each studied vessel tree geometry)

Node	**Normal vascular tree**		**Vascular system with aneurysm**		**Vascular system with stenosis**	
	Blood pressure [*Pa*]	Blood Flow $[mm^3/s]$	Blood pressure [*Pa*]	Blood Flow $[mm^3/s]$	Blood pressure [*Pa*]	Blood Flow $[mm^3/s]$
N1	3456	27.43	3116	27.42	4404	29.13
N2	2975.82	13.71	2636.00	7.65	3894.17	29.13
N3	2495.64	13.71	2368.20	19.77	2874.53	8.71
N4	2495.64	-1.29	2495.18	-3.62	2569.45	-8.71
N5	2495.64	1.29	2622.16	3.62	2264.38	8.71
N6	2399.60	13.71	2509.11	16.14	2203.36	8.71
N7	2399.60	13.71	2289.25	16.14	2731.61	20.41
N8	1780.17	13.71	1779.99	11.27	1809.82	20.41
N9	1300	13.71	1300	11.27	1300	29.13

The resistance of the blood vessels to blood flow is an important factor which controls the blood flow. The data stored in Table 2.3 confirm this fact. In the case of stenosis, $R_{eff} = 1.51$ and the flow rate has the higher value of 29.13 mm^3/s. In the case of stenosis which has been simulated by blocking the branch B-2-5, a pick of pressure appears at node 7 because the blood flows only through the branch B-2-3.

Results explain the crucial role of small arteries in regulation of a local blood flow. Arteries are known as resistance vessels. They prevent damaging the microcirculation. By the variation of the arterial radius, arteries control the distribution of blood to different tissues. Thus, small changes to arterial radius can exert large effects in resistance and therefore blood flow to an organ. On the contrary, venous resistance is relatively low.

The proposed model allows a reasonable understanding of how the branching pattern affects the vessel resistance and the distribution of the blood pressure and blood flow at any node of the vascular tree.

Concluzii

The purpose of this study was to analyze the blood flow profiles and pressure gradients in small vessels of retinal images.

Blood pressure as well as flow values tended to be decreased in patients with DR and clear differences in the blood flow profiles exist between NHR and DR images. The blood pressure and flow profiles for an asymmetry parameter of 0.4 indicate in the cases of NHR1 and DR2 that the pathological

Chapter III
Digital image enhancement methods

A phenomenon that affects the digital image and the useful information it contains is image noise. This occurs due to the imperfection of the acquisition devices. For enhanced clarity, images can be processed to remove unwanted artifacts. The noise in digital images is of several types [16]: additive, multiplicative, salt and pepper noise, Gaussian noise, white noise and the Rician noise.

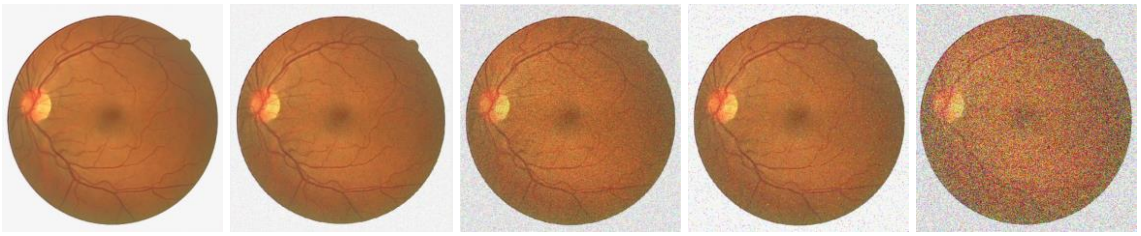

(a) (b) (c) (d) (e)

Figure 3.1 Representation of the influence ofcertain types of noise over an image. (a) original; (b) additive noise; (c) multiplicative noise; (d) salt and pepper noise; (e) Gaussian noise.

The sources of the analyzed retinal images are the DRIVE database [15] of the University of Utrecht. The source of the angiograms is the website Radiopaedia.org [17], which is a member of the UBM Medica network and from Medscape.com [18], which is part of WebMD Health Professional Network.

3.1 Histogram equalization and contrast enhancement

3.1.1 Histogram equalization

Digital images have a complex structure and show uneven gray levels, meaning that in any image there are predominant gray levels and less gray or absent gray levels. The goal of image enhancements is to redistribute the gray levels in the image so that they can handle the full range of available values. If desired, after the image enhancement operation the gray levels or illumination intensities to be uniform, then to achieve this requirement, the histogram equalization operation is required [7]. Image

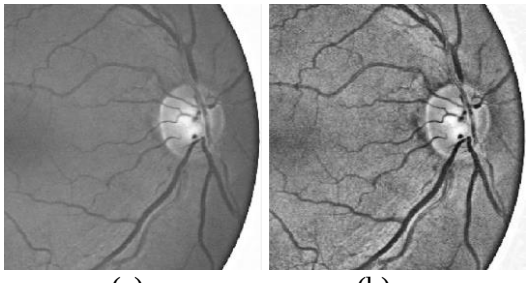

(a) (b)

Figure 3.2 Representing the histogram equalization method by adaptive contrast limiting filtering. (a) original; (b) CLAHE.

improvement by enhancing contrast with histogram equalization, is one of the main techniques used in image processing.

Contrast-Limited Adaptive Histogram Equalization (CLAHE) is based on a generalization of normal and adaptive histogram equalization, and is used to locally enhance contrast in images [19].

3.1.2 Contrast enhancement

Image contrast enhancement are transformations that target gray levels and correlate the gray level of the original image with its new values in the processed image.

Linear Contrast Adjustment linearly expands the original pixel values into a new range so that the entire field of sensitivity is used. Both the new maximum and minimum thresholds are defined in order to make use of the entire range of available brightness values [20].

3.2 Image filtering

The main method used to improve an image by removing the noise overlapping useful information is the filtering operation. For calculating the new pixel value, the filtering operation uses not only its old value, but also the values of neighbor pixels based on mathematical correlation operations [16]. Filtering operations can be performed in the spatial, temporal or frequency domains [3]. Spatial filters fall into two major categories: *high pass filters* that are used in smoothing and / or filtering actions to highlight significant variations in object intensity and contours and *low pass filters* used to diminish small intensity variations [6].

3.2.1 Linear image filtering

This method is an operation built on the principle of linearity or superposition. This determines the intensity of each pixel in the filtered image based on a linear combination of neighbor pixel values (placed in the selected mask) in the original image [21].

Types of linear filters are: Blur Filter, Sharpen Filter, Bias correction, Laplacian filter, Gaussian filter, Laplacian&Gaussian (LoG), Marr-Hildreth and Wiener filter.

3.2.2 Nonlinear image filtering

Nonlinear filtering falls within the category of interdisciplinary analyzes, that are capable of delivering images whose quality exceeds the limits imposed by the acquisition systems. A particular characteristic of this type of filtering is the Bayesian probabilistic property. Bayesian learning uses the concept that quantitative elements are directly determined by the probabilities distribution. It combines the information theory, stochastic analysis and statistics. This method has a wide spectrum of applicability, being an extremely robust tool in imaging and video processing, speech processing and recognition, genetics, Bayesian networks and others [16]. Nonlinear image filtering types are: median filter and maximum and minimum filter.

3.3 Wavelet transform

In recent years, multi-resolution analysis techniques, especially those based on the use of the Wavelet transform, where expanded. Due to the special attention given to this methods, it has been successfully expanded into various fields of activity such as telecommunications, geophysics, medicine, astronomy, forensics, etc. As examples of applications we can include studies for biomedical signals and noise filtering in images. Generally, wavelet transforms allow the decomposition of complex signals into sums of basic functions [22]. The implementation of wavelets in filtering algorithms is difficult because of the very complex mathematics [23]. From a mathematical point of view, wavelet transform presents the following properties [1]: has null and is centered around t = 0.

3.4 Fourier Transform

Fourier transform is an alternative method to linear filtering, that allows image processing with certain frequencies [24]. Depending on the intended purpose, the Fourier transform can be built with low pass filters for smoothing and noise removal or with high pass filters for edges enhancement.

3.5 Quality descriptors

Numeric quality descriptors serve to analyze processed images and are computed by reference to the original image quality. The most commonly used descriptors are: Signal to Noise Ratio (SNR), Contrast to Noise Ratio (CNR), Mean Square Error (MSE), Root Mean Square Error (RMSE), Peak Signal to Noise Ratio (PSNR), Mean Absolute Error (MAE), Correlation coefficient (CoC), Bhattacharyy coeffcient, relative entropy (mutual information), Structural similarity index (SSIM), Mean structural similarity index metrics (MSSIM), Quality index based on local variance (QILV) and Feature Similarity Index (FSIM). In order to evaluate the quality of an image, quality measures are used which are 2D extensions of the images subjected to quantification [21].

3.6. Image binarization

Image binarization operation aims for a black and white image, from one containing other unwanted hues from various technical reasons.

3.6.1 Binarization by thresholding

This type of binarization, based on a chosen optimal threshold, is often used in the image segmentation operation based on the intensity or color analysis of each pixel. Binarization can be done with a global or local threshold set for each subdivision of the image [25]. The most commonly used binarization methods are:

- Fisher method, where the optimal partition minimizes the inertia of classes relative to their average.
- The Bhattacharyya method involves histogram decomposition [25].

- The Otsu method, when optimal partition minimizes one of the ratios between the partition variance and the global variance. The method is based on the fact that minimizing variance within the class leads to maximizing variance between them [26].

3.6.2 Region-based segmentation

This method uses the analysis of belonging criteria of a pixel or region to a target object. The criteria used may be the average value of the illumination, color or texture of the region or object being analyzed. Region-based segmentation can be done with three methods:

- Segmentation based on region growth - in this case it starts from a point (pixel) and iteratively analyzes the adjacent points.
- Splitting - the operation starts from a large area, which may be the entire image. This is divided into several regions.
- Split & merge - splitting the image into smaller, usually fixed-sized regions. Merging regions is based on criteria met by edge pixels. [27]

3.7 Personal contributions

3.7.1 Assessment of vessel diameters for MR brain angiography processed images

The images used are MR images of the cerebral circulatory system of different patients. The source of the angiograms is the website Radiopaedia.org [17], which is a member of the UBM Medica network and from Medscape.com [18], which is part of WebMD. The images used are MR images of the cerebral circulatory system of different patients. The image processing was performed with a series of algorithms, developed and in MATLAB. This study compares the vessel diameters from the acquired original MR brain angiography images and processed images. The purpose of this study was to determine which one of the techniques presented, represents the best way to improve a MR brain angiography image.

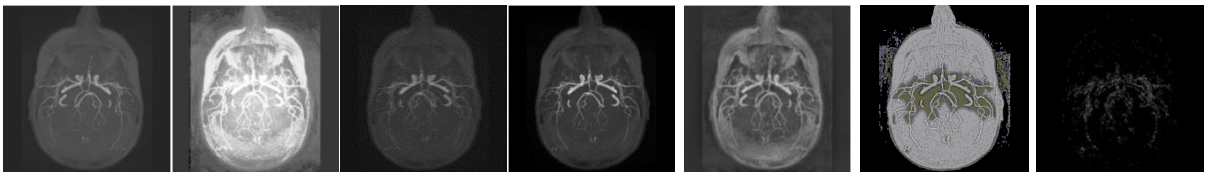

(a) (b) (c) (d) (e) (f) (g)

Figure 3.3 Original and processed MR brain angiography.(a) original image; (b) histogram equalization (HE); (c) Wiener filter (WF); (d) linear contrast adjustment (LCA); (e) contrast-limited adaptive histogram equalization (CLAHE); (f) Bias correction (BE); (g) Marr-Hilderth filter (MHE).

The following techniques: histogram equalization (HE), Wiener filter (WF), linear contrast adjustment (LCA), contrastlimited adaptive histogram equalization (CLAHE), bias correction (BC) and the Marr-Hildreth filter (MHF).

In the figure 3.4 a comparison between the relative errors in every image has been made. The smallest error is generated by linear contrast adjustment (LCA) and the largest by the Marr-Hilderth edge (MHE). Also, we can observe that the other processing techniques are not returning consistent results. HE performance is affected by the loss of definition on the edges and over enhancement of noise in the image; the error generated by this technique is between 0.09 and 0.22. Because of this drawback the relative error of this algorithm is not consistent; the difference between the lowest and the highest error is too large.

Like the HE, the Wiener filter (WF) is not consistent either. The errors vary between 0.05 and 0.21 and the variation in this case is even larger. Despite this, the WF generates smaller relative errors than histogram equalization. The errors generated by the LCA algorithm range between 0.02 and 0.04, so the enhanced images generate results close to the original MR image. Moreover, the results are very consistent, with a small difference between the lowest and highest relative error. The CLAHE method has errors ranging between 0.05 and 0.15 and produces smaller variations than WF, and smaller errors than both HE and WF. BC generates relative errors between 0.04 and 0.14.

Compared to the HE, WF, CLAHE and MHE algorithms, the generated errors are smaller and the results are closer to the original image. MHE algorithm generates the highest errors, and also, in absolute numbers, it generates the largest variation between resulted errors. The relative errors generated by MHE are situated between 0.35 and 0.57. Overall, theLCA algorithm was found togenerate better results. Some limitations of this study could be highlighted.

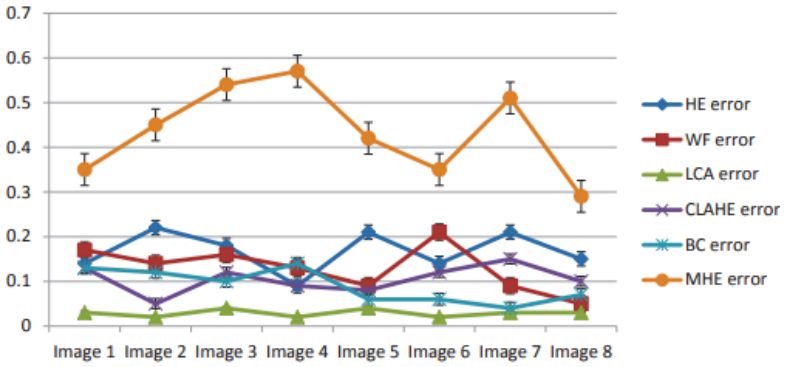

Figure 3.4 Comparison between relative errors generated by processing techniques

Thus, age and gender or the image quality and the general image artifacts such as noise can affect the vessel dimension. Also, here only a single angiographic projection has been used. The main conclusion of this study is that linear contrast adjustment represents the technique that generates the smallest relative error and the closest value to the true value. Also, it is the most constant processing technique, unlike the other proposed algorithms.

3.7.2 A survey over image quality analysis techniques for brain MR images

Despite of the multiple advantages offered by MRI technique, it shows some pitfalls as the noise presence or the non-standardized intensity, namely the MRI pixel intensities have no fixed value on the targeted tissue.

To overcome these drawbacks, various images processing tools and methods had been proposed. According to the information provided in Table 3.1, the most frequently used objective metric in the evaluation of the quality of processed MR image is SNR. The reason is that SNR is slightly tissue-depended. From the hybrid metrics, the most used is SSIM. If the value of SSIM is close to 1 the analyzed images tent to be similar. The principal objective of this survey was to provide an overview of the available brain MRI metrics and on their applicability and limitations in the evaluation of the quality of the processed images. This paper summarized the objective and hybrids metrics that are HVS-based characteristics. Also, it discusses on the notion of image quality.

Table 3.1 The searched items according to keywords from PubMed Database.

Metric	Searched terms	Number of items
SNR	Signal-to-noise ratio brain MRI	1681
PSNR	Peak signal-to-noise ratio brain MRI	65
MSE	Mean square error brain MRI	85
RMSE	Root mean square error brain MRI	48
MAE	Mean absolute error brain MRI	33
CNR	Contrast to noise ratio brain MRI	695
BC	Bhattacharyya coefficient brain MRI	3
MI	Mutual information brain MRI	246
SSIM	Structural similarity index brain MRI	15
MSSIM	Mean structural similarity index brain MRI	2
QILV	The quality index based on local variance brain MRI	1
FSIM	Feature similarity index brain MRI	5

Conclusions

The studies on existing experimental data, as well as my own experimental research presented in this chapter, were designed to demonstrate that it is possible to use the methods of image enhancement to facilitate and improve the objectivity of the diagnosis of cerebral vascular system and its affections. The analysis of the proposed methods results in the following conclusions:

a) Using algorithms to enhance medical images and to suppress noise that occurred during the acquisition process is an essential step of pre-processing.
b) The use of linear or nonlinear filtering methods can help physicians to make decisions about the diagnosis of different patients for diseases such as diabetes, high blood pressure or the presence of a cerebral aneurysm.
c) Filters used on different angiographic images have the advantage of extracting information from MRI images using clustering algorithms.
d) Quality descriptors, objective or hybrid, can be used successfully in assessing the quality of processed images, by comparison to the original images.

Chapter IV
Advanced segmentation methods

Medical imaging facilitates and improves the accuracy of detection of certain types of illness, such as diabetic retinopathy or cerebral aneurysm. Thus, in order to identify microvascular abnormalities of blood vessels, retinal images are used. Because of uneven illumination of the image, complex background and ocular vascular system asymmetry, measurements are often inaccurate.

For this reason, different methods of edge detection have been developed over the past decades. These methods are used when non-uniform illumination is a factor limiting the detection of various anomalies. These segmentation methods range from simple methods that use threshold methods to complex techniques such as fusion of complex images.

In this section of the thesis, the DRIVE [15] image database for the retinal circulatory system is used and the Radiopaedia [17] database for cerebral vascular system images. Also, processed images are their own images.

4.1 Region-based segmentation

4.1.1 Histogram based segmentation

This technique is a binarization method based on the number of occurrences of gray levels in an image. Histogram-based segmentation methods are constructed on gradient fluctuations, which offer the possibility of using different thresholds. This technique is leading to the separation of the analyzed background objects [28].

4.1.2 Fisher method

The Fisher method is used to find the variance of an estimator using Cramer-Rao inequality, as well as to determine the asymptotic behavior of maximum probability estimation. Thus, for a random variable *x* and $p(x, \theta)$ the probability function for a data model with θ parameter, the Fisher method is maximizing the probability by maximizing the likelihood of the θ parameter [29].

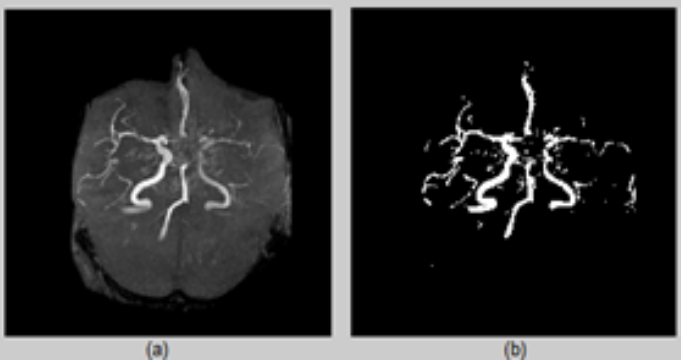

Figure 4.1 Cerebral anneurysm. (a) original image (b) image segmented by Fisher method.

4.1.3 Otsu method

The Otsu method is a thresholding method that performs an image segmentation by separating objects from the image background [30].

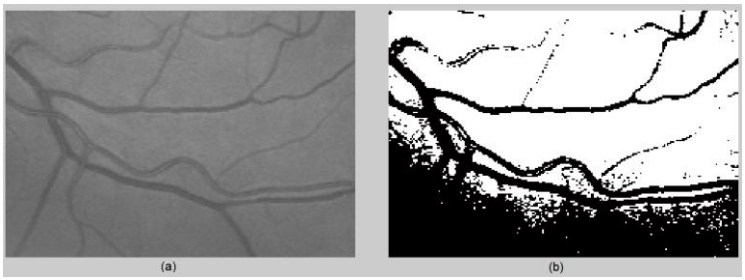

Figura 4.2 Arbore vascular retinal. (a) imagine originală; (b) imagine segmentată prin metoda Otsu.

4.2 Edge detection methods

4.2.1 Sobel method

The Sobel operator measures the gradient of the image in the 2D domain and thus highlights the edges of the objects in the image. Typically, the operator is used to determine the approximate gradient intensity at each point in the gray image [31].

4.2.2 Canny method

Canny filter is considered an optimal edge detector as it provides the lowest error rate in the real edge point detection. This method works according to the following criteria: decreases the error rate because it does not lose edge points and does not respond to points that are not on the edge; the points moved along the edge are well located, and the detector provides a single response for each point on the edge [32].

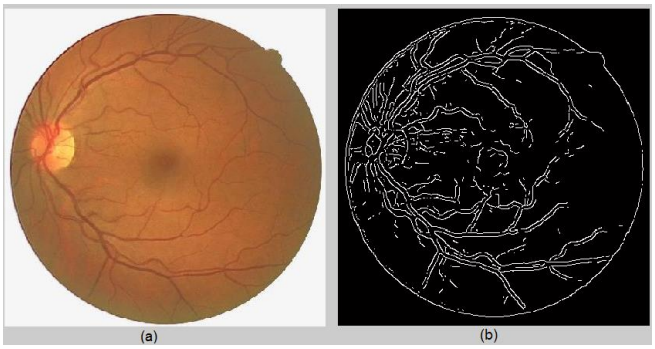

Figure 4.3 Retinal vascular system.
(a) original image (b) segmented image.

4.2.3 Prewitt method

The Prewitt method is an algorithm for detecting vertical and horizontal edges specific to the objects in the image. This is a discrete differential operator that is formed by the convolution of two matrices [33].

4.2.4 Roberts method

The Roberts method for edge detection is based on the image gradient measurement. Specifically, it highlights the spatial regions specific to the highest gradient values, which often correspond to the edges. [34]

4.2.5 Laplacian&Gaussian Filter

The LoG filter is an isotropic spatial filter of the second spatial derivative of a 2D Gaussian function. It convolves an image with a mask and acts as a zero crossing detector in

order to decide which pixels are the edge pixels. It analyses the pixels placed on both sides of the edge and selects those pixels that are closest to the zero-crossing points.

4.2.6 Gabor Filter

2D Gabor filter-based edge detection is based on frequency and orientation representations. It is a Gaussian kernel function modulated by a sinusoidal plane wave oriented at an angle. The function is:

$$G(x) = \frac{1}{\sigma\sqrt{2\pi}} \exp\left(-\frac{x^2+y^2}{2\sigma^2}\right) \exp[j\omega_x(xcos\theta + ysin\theta)] \quad (4.1)$$

where σ is the standard deviation of the Gaussian function in the x and y direction, ω_x is the frequency of a sinusoidal wave and θ is the filter orientation [35].

4.2.7 Frangi Filter

Frangi filter uses information extracted from the Hessian eigenvalues. The filter computes the Hessian matrix by using Gaussian second order derivatives of images [36].

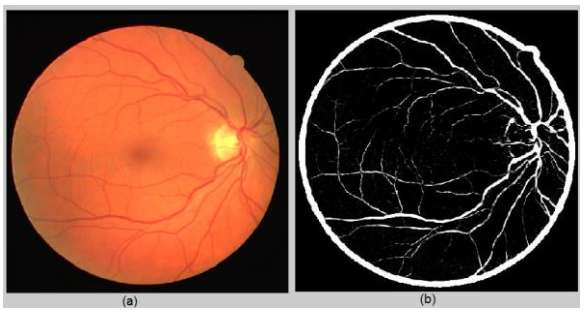

Figure 4.4 Vascular tree edge detection using Frangi filter.
(a) original image (b) segmented image.

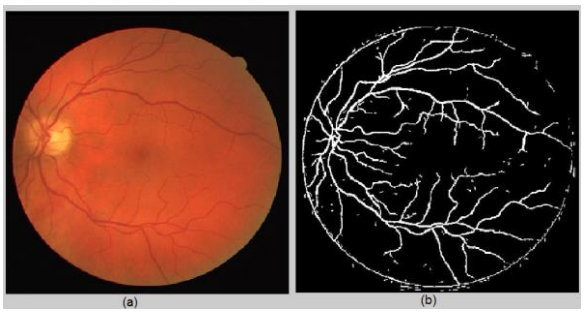

Figure 4.5 Vascular tree edge detection using COSFIRE filter.
(a) original image (b) segmented image.

4.2.8 Cosfire Filter

The COSFIRE filter allows the segmentation and edge detection of the vascular system in retinal images. The output data of the Difference-of-Gaussians (DoG) filter for certain particular positions against the center of the analyzed area [37].

4.2.9 Matched filtering

Represents a method used in medical imaging because it helps for different affections detection. This filter is formed by correlating two signals, a known one and an unknown one in order to detect the chosen template in the second one [38].

4.3 Image fusion methods

4.3.1 Dempster-Shafer fusion for edge detection

The Dempster-Shafer edge detector is based on a mathematical theory of evidence. It is build on the Shafer's framework of belief functions and plausible reasoning and on the Dempster rule of combination that assigns probabilities to the belief functions. The edge detector uses uncertain reasoning to compute the probability of an event by combining different

information sets obtained from previous filtering operations. This theory has spectacular applications in medical imaging. [39]

In order to take advantage of three of the most commonly used filters (Log, Canny and Gabor), we used the Dempster-Shafer theory to combine the images resulting from the previous filters.

Filters are considered evidence for each case. For example, the Canny and Gabor filters are considered evidence, and their results are used as events of the Dempster-Shafer fusion. By fusing them, edge detection is done with greater accuracy.

Another fusion of images was made between the Frangi and COSFIRE filters. Adjustment of weighting was done manually. [40]

4.4 Methods for assessing the quality and accuracy of processed images

4.4.1 Edge-based structural similarity

In order to assess the fusion performance for real edges detection, the edge-based structural similarity (ESSIM) is calculated. It analyzes the structural similarity of images based on the detected edges between the reference/ground truth images (R) and the fused images (F) images [41].

4.4.2 Pratt's Figure of Merit

Pratt's Figure of Merit (FOM) is used to evaluate the performance of the fusion compared to the results of the classical filters. Pratt's FOM analyzes the accuracy of the edge location by calculating the metric of the edge points from a ground truth retinal image and the processed image [42]. 4.5 Personal contributions

4.5.1 Retinal vessel enhancement based on the gaussian function and image fusion

The abnormalities in the vascular system, particularly those of diabetic retinopathy disorders, demand accurate measurements, and both the asymmetry of vessels and the complexity of the background generate inaccurate measurements [43].

50 retinal images from the DRIVE digital retinal images were analyzed [15]. The database consists of 25 randomly selected images and 25 manually segmented images used as ground truth. They were divided as follows: 15 belong to healthy

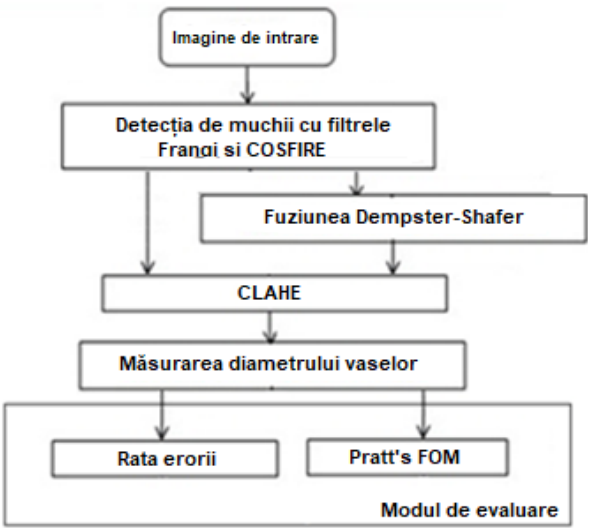

Figure 4.6 Flow chart of the proposed

patients and 10 are diabetic retinopathy retinal images. The flow chart of the proposed method is presented in figure 4.6. The performance of the DS fusion against the Frangi and COSFIRE filters is evaluated by measuring the diameter of the retinal vessels. The diameters of the segmented vessels were measured using a homemade algorithm implemented in Matlab.

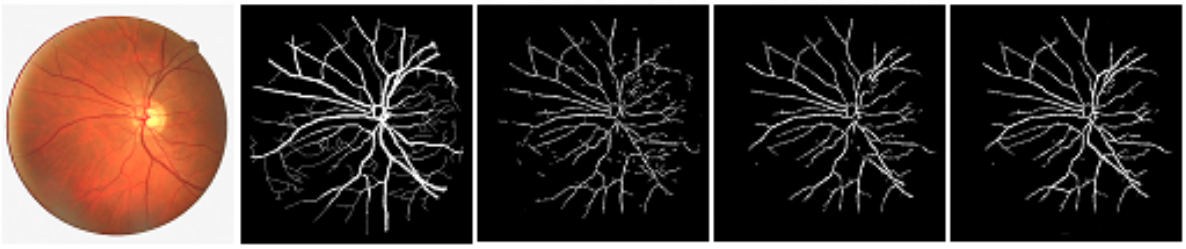

(a) (b) (c) (d) (e)

Figure 4.7 Examples of vascular map. (a) Original input image; (b) ground truth image (manually segmented); (c) Frangi filter; (d) COSFIRE filter; (e) Dempster-Shafer fusion.

Table 4.1 The average vessel diameter values and the average percentage error, for normal (N) and diabetic retinopathy

	Ground truth	FF	e_{FF}%	CF	e_{CF} %	DS	e_{DS} %
N	5.34	4.98	6.74	5.66	5.99	5.09	**4.68**
DR	5.64	5.89	4.43	5.96	5.67	5.41	**4.08**

In order to evaluate the performance of the proposed fusion algorithm compared to the classic filters, measurements were conducted on 25 randomly selected retinal images. Table 2 displays the quantitative measures of the performance through the average Pratt's FOM. It can be observed that DS detected edge map images have higher Pratt's FOM values. On the other hand, COSFIRE detected edge map results in lower Pratt's FOM values

Table 4.2 Retinal vessel enhancement based on the Gaussian function and image fusion

	FF	CF	DS
N	*0.9612*	*0.9589*	***0.9768***
DR	*0.9621*	*0.9618*	***0.9782***

Table 4.1 presents the mean values and percentage error of vessel diameters for manually segmented, filtered and fused retinal images. For images segmented with classic filters, the smallest errors are generated by the Frangi filter (FF) for diabetic retinopathy samples, and COSFIRE (CF) for healthy subjects. According to data in figure 2, Frangi and COSFIRE filters can often lead to false edges or to edges that are shifted or doubled. On the other hand, DS fusion generates better results and smaller errors than classic filters.

In table 4.2, the Pratt's FOM results provide another edge detector performance assessment. It balances the ideal (or good) edges with the effect of erroneous edges in filtered images. The highest edge similarity between an ideal edge map provided by manually segmented images and the detected edge map is obtained for DS fusion, for both healthy and diabetic retinopathy images. Comparing the results in table 4.2, we can see that the difference between ground truth and filtered images is less than 5% for both edge detectors, and less than 3% for fused images.

DS fusion searches for a compromise between these two edge detectors in the field of edge maps so that there is no over-edge detection via this method, and the edges are more continuous. Another observation is that the Pratt's FOM values for diabetic retinopathy images are slightly higher than those computed for healthy patients.

The DS fusion between output images given by Frangi and COSFIRE edge detectors generates better results than any of them used alone, for both healthy and diabetic retinopathy retinal images.

4.5.2 Comparative assessment of retinal vasculature using matched filtering

Matched filtering is used in medical imaging because it helps for different affections detection. This filter is formed by correlating two signals, a known one and an unknown one in order to detect the chosen template in the second one [44].

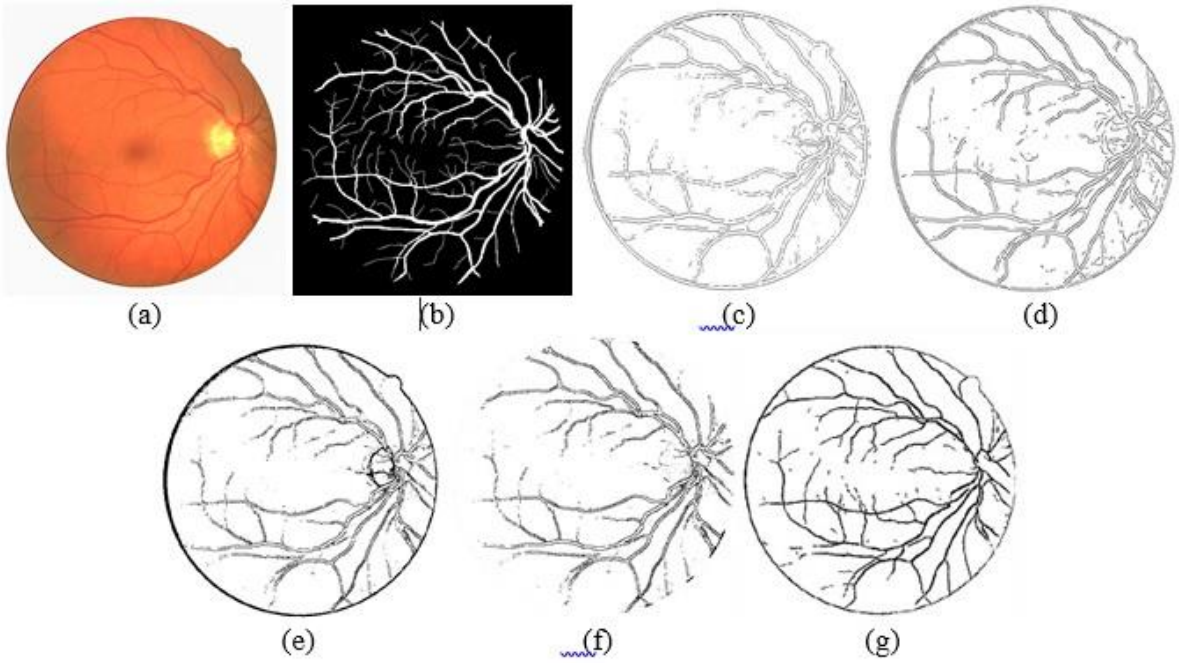

Figure 4.8 Examples of vascular map. (a) Original input image; (b) ground truth image (manually segmented); (c) LoG filter; (d) Canny filter; (e) Gabor filter; (f) Frangi filter; (g) Matched filter

This study aims to determine the accuracy of a vascular map generated by a matched filter compared to classical filters in retinal images. The performance of four classical edge detection methods and of a matched filter is assessed. In order to evaluate the performance of the algorithms tested in this study, measurements were conducted on 30 randomly selected images. Figure 4.8 shows retinal vascular maps generated by the classical filters and matched filter. For a more profound result the diameter of the vessels was computed for normal patients and those with diabetic retinopathy.

Table 4.3 The average vessel diameter (DM) values and the average percentage error (E%), for normal (N) and diabetic retinopathy (DR)

		Referința/segmentare manuală	**LoG**	**CF**	**GF**	**FF**	**MF**
N	**DM**	4.91	4.48	4.61	4.53	4.59	4.67
	E (%)	-	8.75	6.11	7.73	6.51	4.88
DR	**DM**	5.02	4.62	4.71	4.66	4.74	4.79
	E (%)	-	7.96	6.17	7.17	5.57	4.58

Table 4.4 Comparison of average Pratt's FOM for normal (N) and diabetic retinopathy (DR)

	LoG	**CF**	**GF**	**FF**	**MF**
N	*0.9448*	*0.9602*	*0.9464*	*0.9612*	*0.9694*
DR	*0.9455*	*0.9634*	*0.9481*	*0.9621*	*0.9712*

Table 4.3 presents the retinal vessels diameter and percentage error values for the manually segmented retinal images and for those filtered using classical filters and matched filter. The classical filter that generates the most accurate result for retinal images of normal patients is Canny filter, with an error of 6.11%, and for those with diabetic retinopathy the Frangi filter with an error of 5.57%. Furthermore, the percentage error generated by Canny for diabetic retina is 6.17% and an error of 6.51% for retinal images is established for Frangi filter. Between these two filters equilibrium is noticed, with comparative results and relative low error rates, with the mention that Frangi filter generates the most continuous edge maps between the classical filters. The worst results characterized by the largest error rates for both normal patients and diabetic patients are provided by LoG filter, with errors of 8.75% and 7.96% respectively. The Gabor filter generates relatively large error values, but it has to be mentioned that it generates continuous edge maps.

In table 4.4, the results generated by Pratt's FOM are displayed. They were generated after comparing the ground truth edges with those presented in the processed images. The

highest similarity of the edges is obtained for Matched filtering with a dissimilarity degree from the ground truth images of 3%, for both normal and diabetic retinopathy subjects. The diference betweent the manually segmented retinal images and the processed ones is less than 4% for Canny and Frangi filters and less than 6% for LoG and Gabor filters.

4.5.3 Dempster-Shafer fusion for effective retinal vessels' diameter measurement

This paper focuses on the selection of the best combination of methods dealing with edge detection, when the uneven surface illumination is a limiting factor, by using image fusion. The fusion overcomes the drawbacks of simple edge detection methods and provides a more accurate vascular map of retinal images.

So, in this paper, we investigate the performance of the some edge detection algorithms coupled by image fusion technique. The key contributions of the work are as follows. 1) The source images are the regions of interests (ROIs) selected from uniform, moderate and low levels of illumination over image edge sites. 2) Laplacian of Gaussian (LoG), Canny (C) and Gabor (G) filters were used for primary edge detection. 3) DS method fuses paired filtered images. 4) CLAHE (contrast limited adaptive histogram equalization) method was used to improve the results of fusion. 5) The improvement brought by data fusion is evaluated by conducting measurements on the diameter of the retinal vessels. A homemade algorithm was developed using Matlab. Also, the ImageJ plugin was used for this experiment. The segmented retinal images provided by DRIVE database were used as ground truth images. The accuracy of the proposed edge detection method was analyzed by means of edge-based structural similarity metric (ESSIM) that compares all detected edge pixels with the true edge pixels of ground truth images.

The proposed method was tested on the public digital retinal images for vessel extraction (DRIVE) dataset consisting of 30 randomly selected retinal images and 30 manually labeled images as ground truth [15]. From these, 36 are normal and 24 are affected by diabetic retinopathy.

In this paper we address to the problem of luminance fluctuations mainly due to the spherical geometry of the eye and the interaction between illumination and specular reflection produced by various anatomic parts of retina. To analyze the influence of uneven illumination, three ROIs from different sites of retinal images have been chosen: 100% or uniform level, 80% or moderate level and 60% or low level. The ROIs size is 100×100 pixels.

To measure the retinal vessel of interest, an essential step is to detect and segment the vessels. In order to keep a balance between accuracy and the cost of operations, LoG, Canny and Gabor filters were selected as edge detection operators. The output images of the LoG, Canny and Gabor edge detection operators represent the input images for the fusion operation.

The LoG filter meets the following conditions: a mask, [0,1,0; 1, -4.1; 0,1,0] and size 3x3. The Canny edge detector uses a convolution mask: [2, 4, 5, 4, 2; 4, 9, 12, 9, 4; 5, 12, 15, 12, 5; 4, 9, 12, 9, 4; 2, 4, 5, 4, 2].

The performance of the proposed fusion method is evaluated by conducting measurements on the diameter of the retinal vessels. Frequently, the detected edges are not always thin (2-3 pixels) or some edge detectors detect double edges in the case of one-pixel-width edges. To overcome these drawbacks, the vessel diameters were automatically measured using two methods. One consists of a homemade algorithm using Matlab and the second uses the facilities of the ImageJ.

For LoG and Gabor filters, the establishment of the threshold involved the use of different images with different attributes and the optimal threshold has been selected based on visual assessment. Canny filter automatically assigned both threshold values.

Figure 4.9 shows some examples of vascular map generated with the D-S fusion of the images provided by pairs of filters and for various illumination conditions. The value of the weight coefficient of the D-S evidence combination is w = 0.32.

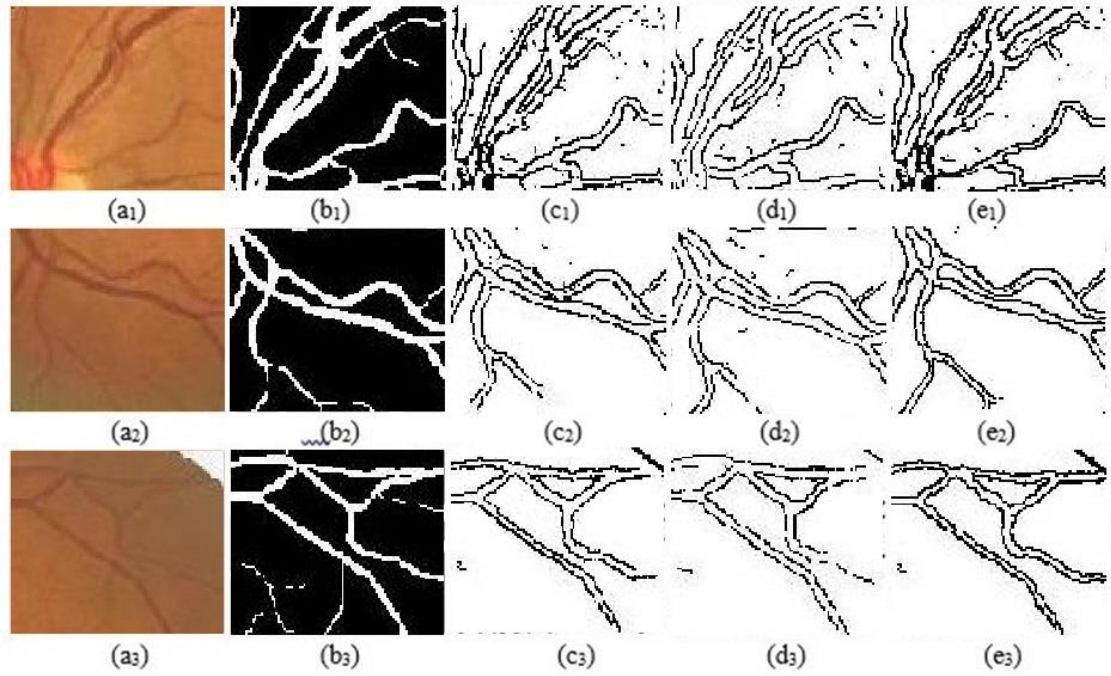

Figure 4.9 Examples of vascular map generated with the D-S-based edge detector fusion, where (ai) RGB (Red-Green-Blue) input images of size 100 × 100 pixels; (bi) ground truth image (manually segmented); (ci) D-S fusion for C-G; (di) D-S fusion for C-LoG; (ei) D-S fusion for G-LoG

For the entire dataset, the accuracy rate for vessel diameter measurement is given in table 4.5 for every fused pair of edge detectors and illumination level.

Tabel 4.5 The average percentage error rate (%) for the vessel diameter measurements

		$e_{C\text{-}G}$%	$e_{C\text{-}LoG}$%	$e_{G\text{-}LoG}$%
100% illumination	Matlab	3.30	5.07	5.94
	ImageJ	3.86	5.18	8.02
80% illumination	Matlab	6.26	5.65	7.17
	ImageJ	8.38	4.85	11.56
60% illumination	Matlab	4.70	11.01	10.64
	ImageJ	5.24	14.52	8.33

Figure 4.10 shows the quantitative performance measures through the average ESSIM and its statistical analysis between the manual segmented image (ground truth) and the fused images. Typically, a very good edge similarity is shown if the ESSIM has a value close to1. Slightly higher values of the ESSIM have been observed for diabetic retinopathy images.

Table 4.6 The average vessel diameter values and the average percentage error using Matlab for healthy (N) and diabetic retinopathy (DR)

		Ground truth	C-G	$ER_{C\text{-}G}$ %	C-LoG	$ER_{C\text{-}LoG}$ %	G-LoG	$ER_{G\text{-}LoG}$ %
100% illumination	N	5.01	5.07	3.35	5.13	5.01	5.14	5.78
	DR	5.09	5.05	3.07	5.04	5.41	5.22	6.72
80% illumination	N	4.66	4.95	6.42	4.80	6.01	4.93	6.17
	DR	4.74	4.98	5.44	4.92	3.85	5.29	12.18
60% illumination	N	4.22	4.31	3.01	4.64	11.43	4.61	11.14
	DR	4.93	5.05	3.18	5.10	8.93	5.07	8.15

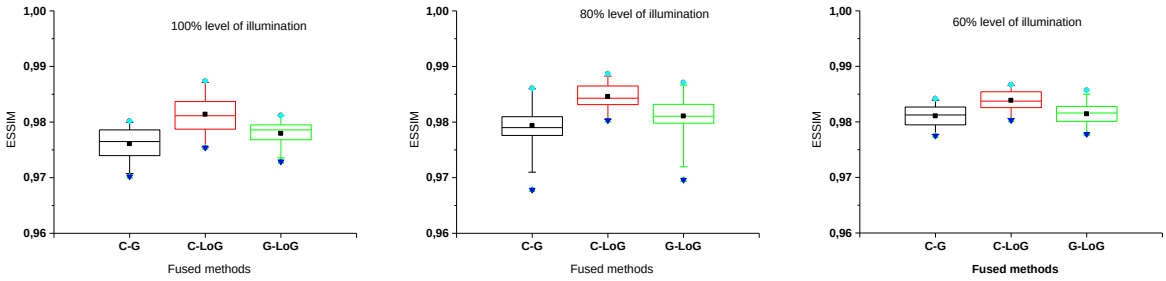

(a) (b) (c)

Figure 4.10 Comparison of average ESSIM using the Matlab framework, for the whole database

Table 4.7 The average vessel diameter values and the average percentage error using ImageJ for healthy (N) and diabetic retinopathy (DR)

		Ground truth	C-G	$ER_{C\text{-}G}$%	C-LoG	$ER_{C\text{-}LoG}$%	G-LoG	$ER_{G\text{-}LoG}$%
100%	N	5.16	5.24	1.96	5.30	8.41	5.46	10.16
illumination	DR	5.21	5.15	1.09	5.30	2.64	5.75	9.70
80%	N	4.67	5.09	10.69	4.92	6.46	5.17	13.80
illumination	DR	4.99	5.61	14.52	5.10	2.40	5.56	12.99
60%	N	4.79	4.99	6.47	5.59	18.60	5.12	8.80
illumination	DR	4.24	4.60	8.64	4.93	18.82	5.13	19.80

This paper is concerned with the D-S theory of evidence adapted to aggregate three independent sources that cover both spatial and frequency domains into one new body of evidence in an edge detection framework. The effect of uneven illumination is taken into account. In the proposed approach, the advantage of the D-S fusion algorithm is considered to generate more accurate edge maps showing almost continuous edges.

Table 4.5 shows the percentage error in vessel diameter measurement. The smallest errors are generated by the C-G fusion for the minimum (60%) and maximum levels of illumination (100%), and by C-LoG fusion for the medium level of 80%. Also, for both algorithms used for diameter measurements, the most consistent results and the smallest errors are generated for images with the highest illumination, and the most inconsistent results for the low level.

A complementary way to asses the performance of paired edge detector operators in detecting real edges (that should be placed in the correct position) is the ESSIM (Fig. 4.10). The highest edge similarity, for every level of illumination, is provided by the C-LoG fusion. C-G fusion provides almost the same results. However, the difference between the ground truth and fused images is less than 3% for all methods and all levels of illumination. When the ESSIM values were computed for normal and for diabetic retinopathy images, those for diabetic retinopathy were slightly higher. This is an expected result because the vessel retinopathy map contains new swollen and distorted vessels that are sources of the new edges. We noted that, even if the neovascularization process is the source of the non-vessel edges such as exudates/bright lesions or reflection artefacts, the fusion technique avoid the false edge detection better that classical edge detectors.

Overall, the C-G fusion generates the better results for high and low levels of illumination and C-LoG fusion is proper for medium illumination. It is worthwhile to mention that this C-G fusion covers both spatial and frequency domains so that the edge detection capability is far better than any one of them used alone. Also, we chose these three edge detectors from a wide range of detection methods because the DS method is suitable only for situations when

all observations have almost the same accuracy estimates. All analysed edge detectors are in compliance with this requirement.

Conclusions

Medical imaging analysis allows the detection of health problems, such as vascular aneurysm and diabetic retinopathy. From the results presented in this chapter, the following conclusions can be drawn:

1. Segmentation and edge detection in retinal imaging can result in high accuracy results, however, most of the time, the detected blood vessel edge are discontinuous.
2. Image fusion is a viable alternative method for classical segmentation methods, because is less affected by uneven illumination, artifacts, or noise in the image. In this case, the edges are much more continuous.

Chapter V
Statistical methods used in the analysis and classification of medical images

Over the past decade, due to the increase in the size and applications of databases in various areas such as commercial, industrial or medical, users interest in automatically extracting knowledge from them, increased also. [45]

Statistics are a set of methods used to gather, describe, and analyze numerical data. It focuses on what can be counted, measured or quantified. Some statistical processing is allowed because there is a possibility of using a numeric coding, even if not all aspects of an object are numeric. Software applications dedicated to statistical processing sometimes require numerical coding for the non-numerical object studied. [46]

5.1 Classification

Classification represents grouping entities in classes of similar entities, considering certain requirements. This can be done manually or automatically. When the classification is done manually, the one who does it works with similarity criteria. As with manual grouping, reasoning is also used for automated methods, so there are two types of automatic classification: predictive and descriptive.

5.1.1 Predictive classification

To explain the predictive classification, we consider two sets Π_1 and Π_2, each being defined by the distribution of the variables. In order to achieve the classification, we must establish the group to which an observation belongs, characterized by the values of the objects considered [47].

5.2 Distances between objects

5.2.1 Nearest neighbor method

The distance between two groups of objects is the minimum distance between two elements of it, namely the distance between the closest elements in different classes. [48]

5.2.2 Farthest neighbor method

This method uses the calculation of the distance between two groups based on the maximum distance between two elements of the groups, namely the distance between the most distant elements of different classes [48].

5.2.3 Average linking method

For this method, the distance between two groups represents the mean distance between group pairs.

5.3 Dendrogram

Clustering technique establishes if two objects are similar or dissimilar by grouping them into clusters. The goal of clustering is descriptive and it groups objects into subsets in such manner that similar objects are grouped together, while different objects belong to different groups. The task of grouping similar objects is accomplished using distance and similarity measures (ex. Minkowski, Ward). The Ward method uses hierarchical classification by minimizing intracluster variability. After applying an algorithm, the tree is generated as a result of it. The dendogram shows the clustering program, indicating the value at which the classes were joined. This hierarchical aggregation solution produces more cluster solutions. Selecting a cluster is done by horizontally splitting the classification tree for different aggregation distance values. A partition of the classified elements set is obtained, and the partition components represent the classes. [49]

5.4 Classification algorithms

To group datasets, classification algorithms are used. This method is useful for large datasets, each class containing elements with similar features [50].

5.4.1 Clustering algorithms

Clustering methods are important in the classification of various types of data extracted from MR images. However, the groups are not predefined, as is the case with classification. Clustering is realised by finding similarities between data according to the features found in current data [51]. Clustering, as a data mining method, identifies densely populated clusters or regions taking into account distances between objects in large or multidimensional datasets. This method is studied in several areas. Some examples of domains are statistics, automated learning, data mining, medicine, biology or economy [52].

Database segmentation consists in grouping a tuples of a database by partitioning or segmenting data into components, which provides the user with an overview of the data.The **k-mean clustering algorithm** selects group centers randomly, followed by assigning points to the nearest center and recalculating the center as the average of this points. In other words, the center of a final class represents a reflection of the characteristics of a representative object of the group [53].

5.4.2 K-nearest neighbors algorithm

This algorithm is a technique that assumes that the entire set of training objects includes both the desired data and classifications for each item. When a new case occurs, the

algorithm checks all data to find the nearest subset of data and gives this subset as a result. [54]

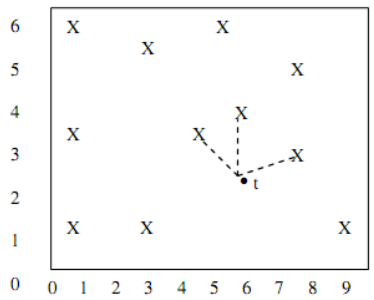

Figure 5.1 K-nearest neighbors representation for k

5.5 Morphological image processing

This type of operations are generally applied to binary images in the preprocessing stage to alter the shape or structure of an object. The main morphological operations are: dilatation, erosion, open and close.

Dilation makes a resizing of the image by realising the links between the discontinuous regions in the image. This operation is accomplished by overlaying and moving a structural element over the image. [55]

Erosion, like dilation, uses a structural element that moves over the image, but this method makes a change of pixels from background objects.

Opening and closing are morphological filtering methods, which combine the advantages of dilation and erosion.

Open represents a sequence of erosion and dilation. This is used to suppress pixels in areas that can not contain a structural element.

Close is a reverse sequence to opening, where dilation is followed by an erosion. This method is mainly used to fill the discontinuities in the image. [55]

5.6 Efficiency assessing methods of classification

5.6.1 t-Test statistical analysis

The t-test method is a deductive statistical test, which determines whether there are differences between the averages of two samples based on p-value. This value p (level of significance) is between 0 and 1 and represents the probability of an error appearance [56].

5.6.2 Dice coefficient

The Dice similarity coefficient performs a qualitative evaluation, and has been used as a statistical validation metric to evaluate the performance of segmentation methods. To evaluate the proposed morphological-based binarization algorithm, the results of the manually segmented images from of the DRIVE database has been considered the ‘ground truth’ or ‘gold standard’. [57]

5.7 Personal contributions

5.7.1 Assessment of the retinal vascular system measurement methods over retinal images from the DRIVE database

The database used for this research consists of 40 RGB retinal images and 40 manually segmented images downloaded from the publicly available DRIVE database. [15]

This study focuses on the assessment of the measurement accuracy of the retinal vascular system’s area by using two algorithms. The research strategy goes through the

following three steps: conversion of the images from RGB to gray scale; a morphological based image binarization; computing the retinal vascular tree's area of interest by counting the white pixels over the region of interest.

Morphological-based image binarization algorithm

The morphological operations work on binary images, because they rely on the relative ordering of pixel values, not on their numerical values.

In the proposed algorithm, the morphological opening operation was used, which is an erosion followed by a dilation, with the same structuring element used for both operations. Two disk shaped structuring elements (2 and 3 pixels respectively) were considered.

Measurement of the area of interest is realised by using two algorithms that allow to crosscheck the value of the measured areas. Also, the same investigation is made over the manually segmented images. Both algorithms follow the same three steps: (i) eliminating the Rician noise from the morphological segmented images, (ii) threshold binarizition, and (iii) computing the area of interest.

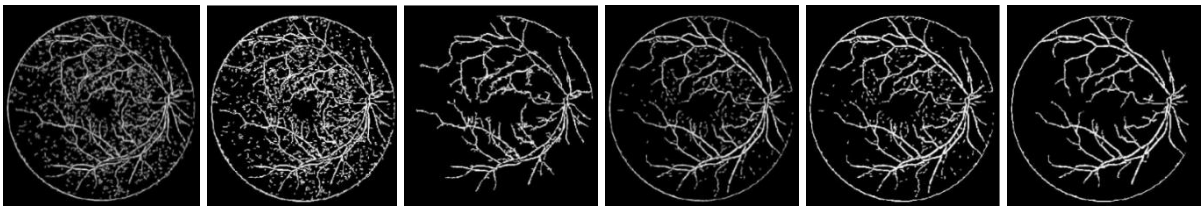

(a1) (a2) (a3) (b1) (b2) (b3)

Figure 5.2 Segmented retinal images after morphology-based binarization algorithm and after steps (i) and (ii) from algorithm 1 and algorithm 2: (a1) segmented image with disk value of 2 pixels; (a2) algorithm 1; (a3) algorithm 2; (b1) segmented image with disk value of 3 pixels; (b2) algorithm 1; (b3) algorithm 2

Table 5.1 Values of the Dice similarity coefficient and standard deviation for algorithms tested using the DRIVE database images

Threshold values		Algorithm 1		Algorithm 2	
		Strel parameter=2	Strel parameter=3	Strel parameter=2	Strel parameter=3
0.25	Dice	0,852	0,897	0.881	**0.919**
	SD	0.116	0.093	0.089	0.062
0.30	Dice	0,855	0,898	0.864	**0.905**
	SD	0.111	0.089	0.095	0.067
0.35	Dice	0,853	**0,895**	0.819	0.878
	SD	0.108	0.087	0.094	0.069

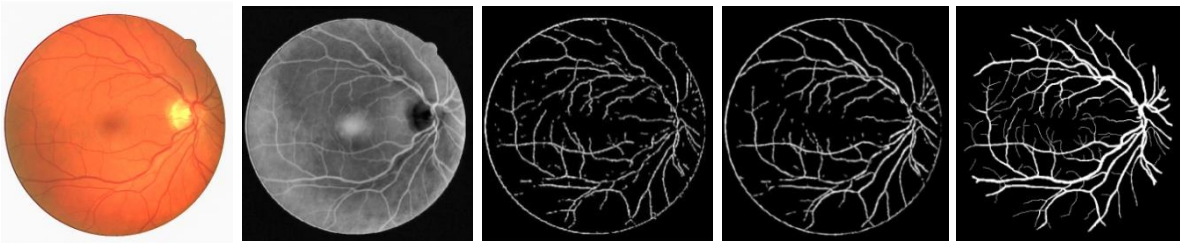

Figure 5.3 Vessel detection for DRIVE database images. (a) original RGB retinal image; (b) grayscale retinal image; (c) binarized image, strel parameter of 2; (d) binarized image, strel parameter of 3; (e) manually segmented retinal image

Algorithm 2, coupled with the disk strel of 3 pixels, shows the higher accuracy. It is more suitable for segmenting the small vascular vessels in retinal images, since the resulted blood vessels network contains almost all the structure of the blood vessel tree. The decrease in the measurement consistency in the rest of the cases indicates that the retinal vessels are not properly detected and the artifacts still influence the measured area value.

The performance of the analysis of the binary images strongly depends on the choice of the proper threshold values. The experimental data suggest that the threshold values of 0.25 and 0.30 return the best results.

The main advantage of our algorithms is the small number of parameters defined in the code. In fact, we defined only the size and shape of the structuring element and the value of the binarization threshold. Furthermore, by using algorithm 2 and a disk strel of 3 pixels, we were able to reduce the information loss in the processed images.

5.7.2 The accuracy of retinal vessel diameter measurement based on pixels distribution and fractal representation

The starting point of this study is based on the finding that line detection methods are reliant and do not provide acceptable results for various experimental conditions. Thus, we compare the vessel diameter values from three datasets, namely healthy, diabetic retinopathy and hypertensive subjects. The goal of this research was to determine if there are any differences between the retinal vessels diameter values of the studied subjects.

Sixty retinal images were used in this research. The sources of the retinal images are the IMAGERET project of the Industrial Engineering and Management from the University of Technology Lappeenranta [13], the database of the Edward S. Harkness Institute from the University of Columbia and the DRIVE database [15].

For the **automated diameter measurement** the following steps are used:

- the retinal image is accessed using the ImageJ plug-in;
- a ROI where the retinal vessel is not distorted and does not overlap another vessel is selected [59];

- the retinal vessel diameter is measured using the 'Set Scale' function. This process involves the calibration using a single image with known values of vessel width. The calibrated image is applied over the unknown images which are measured in an identical manner. In order to achieve this task, the analyzed images must have the same size [17].

Diameter measurement based on histogram with ImageJ software, used the 'Profile Plot' function. This function displays an intensity chart along a line freely chosen in the same location and over the same retinal blood vessel. The representation is made in a xy - coordinate system, where x-axis is the distance along the line and y-axis is the intensity of the pixels. [60]

Diameter measurement based on fractal representation used the 'Surface Plot' function from the ImageJ plug-in. A three-dimensional graphical representation of the retinal vascular system based on the intensity of the pixels in the image has been used to measure the vessel diameter by fractal representation. [61]

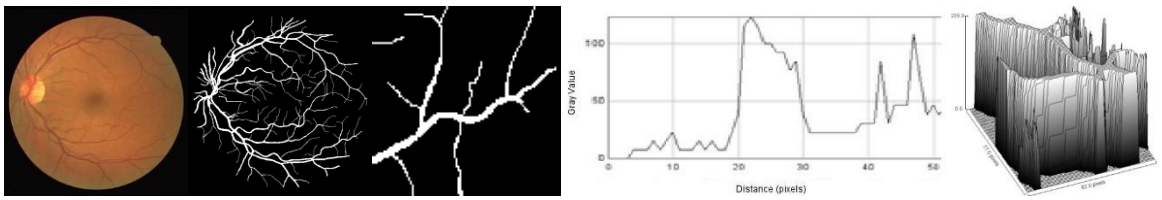

(a) (b) (c) (d) (e)

Figure 5.4 Original and segmented retinal images. (a) original image; (b) binary image; (c) Selected ROI for diameter measurement; (d) intensity histogram of the cross section; (e) fractal analysis.

An example of images used are presented in figure 5.4. The goal of this research was to determine if there are any differences between the retinal vessels diameter values of healthy subjects and those affected by diabetic retinopathy and hypertension.

The reported results indicate that analyzed methods generate slightly different results. Also, the reported values have a small variance. Another observation is that regardless of the measurement method we use, the t-test shows that between the retinal vessels of healthy, diabetic retinopathy and hypertensive subjects measurable differences exist.

According to our analysis, the diameter of retinal vessel is a possible biomarker able to differentiate between healthy subjects and those subjects affected by diabetic retinopathy or hypertension.

5.7.3 A Survey over image quality analysis techniques for brain MR images

This section presents an extension of the studied statistical methods, a study on brain MRI images, which will be further developed in future research.

The proton-density (PD) and high signal intensity T2-weighted (T2w) images belonging to the free Whole Brain Atlas (WBA) database were analyzed. These images are grouped into healthy (HP) and multiple sclerosis (MS) classes. A total of 40 brain MR images were examined. The content of classes is as follows: the first class consists of two axial T2w and PD image series, for two healthy subjects (age 76 and 81, 2 female). The number of analyzed image is 10 T2w and 10 PD; the second class has 10 axial T2w and PD images from two patients with multiple sclerosis (age 30 male, and 62 female). The same number of images was analyzed.

The divisive hierarchical algorithm consists of the following stages: (i) initially exists one cluster that encompasses all objects; (ii) this cluster is successively divided into sub-clusters, and so on; (iii) the stage (ii) continues until the cluster structure is reached. The hierarchical methods are presented using the dendrogram. The dendrogram is a branching diagram showing the similarity among a group of objects [63].

The goal was to determine the optimal threshold. The area of white objects in binary image was identified.

A convenient choice to measure the similarity between classes of MR images from healthy and MS disease is the Euclidean distance. Based on PD and T2w images, the main clusters of the dendrograms are formed using the items of the HP and MS classes. The dendrogram combined with a hierarchical clustering algorithm, is used to identify the classes similarity across the default variables provided by the algorithm.

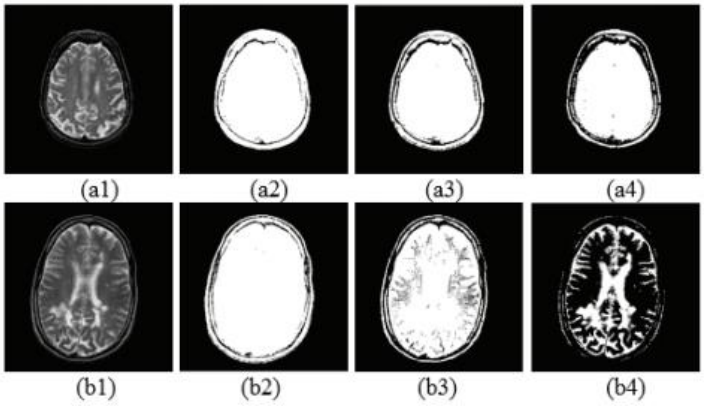

Figure 5.5 Examples of binary segmentation. (a) PD image for a healthy patient; (b) T2w image with multiple sclerosis diagnosis. The first column shows the original image, the second column the binarized images for T=10, the third column the binarized images for T=50 and the forth column the binarized images for T=100.

In our cluster analysis, 20 items started in a cluster on its own and was progressively clustered with others. The optimal number of clusters, according to the linkage criterion, was selected using the criterion of the average distance that computes the average distance between the pairs of points for any two clusters. For both PD and T2w images, the number of main clusters is the same with the number of the studied classes. The nodes on the dendrogram tree represent the internal nodes formed by the linkage algorithm. If the clusters contain the high values of area, the classes HP and MS are joined in a maximum

internal node corresponding to the maximum area. Obviously, the regions that are closest to each other will be eliminated, and those regions that are further apart will remain in the altered data set. In conclusion, the dendrogram is a tool that can separate the HP and PD classes using the dissimilarity between them.

Conclusions

In this chapter, emphasis was placed on the discovery of knowledge related to databases. The experimental data presented in this chapter of the doctoral dissertation allow the following conclusions to be drawn: classification represents a predictive and descriptive object grouping.

- The k-nearest neighbors algorithm has certain advantages, however, in the case of large datasets is affected by inaccuracies in the border area.
- A good method to process a grayscale image is represented by binarization, followed by morphological processing and classification diagrams.

Final conclusions, personal contributions and future research

The research for this thesis was carried out at the Faculty of Science and Environment at the "Dunărea de Jos" University of Galati over a period of three years and aimed at improving, analyzing and extracting information from digital images, about the brain vascular system and retinal circulatory system.

The digital images processing and analysis for use in industry and medicine is an extensive field, and the proposed techniques for extracting information proved able to achieve their intended purpose.

A series of final conclusions can be drawn from the presented information:

- The filters used to process the medical images have the advantage of extracting information from MRI images in spatial, temporal or frequency domains.
- Quality descriptors, objective or hybrid, were used successfully in evaluating the quality of processed images compared to original images.
- Segmentation and edge detection used in retinal imaging provide high accuracy results. For retinal images containing very small vessels, the background noise and the acquired images quality, generates discontinuous blood vessel detected edges and thus some of the information is lost.
- Image fusion is a viable alternative to classical edge detection methods, being less affected by non-uniform illumination, artifacts, or noise. In this case, the detected edges are much more continuous.
- The hemodynamic modeling presented in this thesis represents a step forward in the study of blood circulation in small vessels. Based on my research, blood pressure and blood flow values are decreasing in patients with diabetic retinopathy. Differences are observed between the flow profiles of the images with diabetic retinopathy and those of healthy subjects.

The proposed methods preprocessing, segmenting and performance evaluation are made with the advanced software platforms: Matlab R2014a (Image Processing Toolbox, Wavelets, Graphical User Interface), ImageJ (National Institutes of Health, Bethesda, Maryland) and SPSS 17.0 (SPSS Inc, Chicago, Illinois).

An important and necessary stage in image processing is preprocessing. Using various algorithms, image enhancement and noise reduction are achieved. Also, an improvement in contrast is realised through various algorithms, such as histogram equalization.

Using various filtering methods over angiographic images, we concluded that they can help diagnose diseases such as cerebral aneurysms and hypertension.

In image processing, segmentation and edge detection are essential steps for detecting various disorders of the vascular system. To accomplish these, there are a multitude of established algorithms, such as Canny, Frangi or Gabor.

A contribution to the field of image processing is the fusion algorithm based on Dempster-Shafer mathematical theory. The proposed method is less affected by uneven illumination or image noise compared to conventional edge detection methods. Also, the high similarity between the images generated with Dempster-Shafer fusion algorithm and the original images, as well as the low mean error of vessel diameters, recommend this method as a viable alternative to classical algorithms.

Another important part of the research is represented by the field of hemodynamics. In this research, I conducted an analysis of blood flow and pressure variation in small retinal vessels and differences in blood flow between normal and diabetic human retina. For diabetic retinopathy, the blood pressure and blood flow values are lower than in the case of the healthy retina. Blood flow and parent and daughter vessels provide information that can help evaluate patients affected by vascular disorders.

Although many imaging methods have been developed over the last decades, there is still need for new image acquisition and processing solutions. The research results and the techniques implemented for improving and extracting information from images, were published in prestigious journals, as the Romanian Journal of Physics (IF = 1,759; AIS = 0,243) and a monographic volume in the Elsevier-Academic Press publishing house, three papers communicated and published as ISI Proceedings, in the AIP Conference Proceedings and five BDI papers.

A future direction of research is represented by the image fusion methods for diagnosis of various disorders, such as diabetic retinopathy, hypertension or aneurysm, but also for a deeper understanding of the vascular system pathology. The analysis can be performed using healthy retinal retina / diabetic retinopathy or healthy blood vessel / aneurysm approaches. These modules could be integrated into an automated image processing and analysis system. Another direction of research that can be developed is the processing, extraction of information and the statistical analysis in cerebral MRI images. The first step I made in this direction is presented in section 5.7.3.

Selective references

[1] E. Ceangă, I. Munteanu, A. Bratcu, M. Culea, Semnale, circuite și sisteme, Analiza semnalelor, Editura Academica, Galați, 2001.

[2] C. Vertan, M. Ciuc, Tehnici Fundamentale de Prelucrarea și Analiza Imaginilor, Editura MatrixROM, București, 2007.

[3] R.C. Gonzalez, R.E. Woods, S.L. Eddins, Digital Image Processing Using MATLAB, Prentice Hall, New Jersey, 2004.

[4] C. Grava, V. Buzuloiu, Elemente de prelucrarea și analiza imaginilor, Editura Universității Oradea, 2007.

[5] B. Jahne, Digital Image Processing, The 5th Edition, Springer-Verlag, Berlin, 2002.

[6] J.L. Prince, J.M. Links, Medical Imaging, Signals, and Systems, Prentice Hall, Upper Saddle River, New Jersey, 2006.

[7] C. Vertan, Prelucrarea și analiza imaginilor, Editura Printech, București, 1999.

[8] W. Burger, M.J. Burge, Digital Image Processing, Springer, 2008.

[9] E.R. Weibel, The Pathway for Oxygen, Structure and Function in the Mammalian Respiratory System, Harvard University Press, Cambridge, 1984.

[10] M. Bernot, V. Caselles, J.M. Morel, Optimal Transportation Networks: Models and Theory, Springer-Verlag, Berlin Heidelberg, 2008.

[11] L. Moraru, **C.D. Obreja**, G.E. Monica, S. Moldovanu, Characterization of Vascular Tree: Responses of Blood Pressure and Flow to Branching Patterns with Various Geometries, Annals Of “Dunarea De Jos” University Of Galati Mathematics, Physics, Theoretical Mechanics, Fascicle II, Year VI (XXXVII) Special Issue, 2015.

[12] T. Chacón Rebollo, R. Lewandowski, Mathematical and Numerical Foundations of Turbulence Models and Applications, Birkhäuser 7-44, 2014.

[13] C.D. Murray, The physiological principle of minimum work: I. The vascular system and the cost of blood volume, Proceedings of the National Academy of Sciences 12(3):207–214, 1926.

[14] C.U.I. Jianming, M.A. Jing, Traffic Flow Simulation Model Based on Kirchhoff's Law, International Journal of Digital Content Technology and its Applications (JDCTA) 6(6), 2012. doi:10.4156/jdcta.vol6.issue6.4

[15] Image Science Institute, University Medical Center Utrecht, http://www.isi.uu.nl/Research/Databases/DRIVE/. Accesat: 15.08.2015, 15:12.

[16] M. Ivanovici, Procesarea Imaginilor - Îndrumar de laborator, Editura Universității Transilvania, Brașov, 2006.

[17] Radiopaedia, https://radiopaedia.org/cases/left-middle-cerebral-artery-territory-infarct.

Accesat 7 Dec. 2015, 19:55.

[18] Medscape, http://www.medscape.com/. Accesat 12 noiembrie 2015, 18:42.

[19] Hanan Saleh S. Ahmed, J. Nordin, Improving Diagnostic Viewing of Medical Images using Enhancement Algorithms, Journal of Computer Science 7(12):1831-1838, 2011.

[20] R. Klein, C.E. Myers, K.E. Lee, R. Gangnon, B.E. Klein, Changes in retinal vessel diameter and incidence and progression of diabetic retinopathy. Arch Ophthalmol. 130:749-755, 2012. PMID: 22332203

[21] C. Solomon, T. Breckon, Fundaments of Digital Image Processing, A Practical Approach with Exemple in Matlab, John Wiley & Sons, Chichester, 2011.

[22] P. Porwik, A. L. Haar, Wavelet Transform in Digital Image Processing, Status and Achievements Machine Graphics&Vision 13(2):79-98, 2004.

[23] I.B. Ciocoiu, V. Grigoraş, Tehnici moderne de procesare a semnalelor, Editura CERMI, Iaşi, 2005.

[24] I.W. Selesnick, The double-density dual-tree discrete wavelet transform, IEEE Trans. Signal Processing 52(5):1304-1314, 2004.

[25] Segmentarea imaginilor, Universitatea Politehnică Bucureşti, http://imag.pub.ro/ro/cursuri/archive/12.pdf, Accesat: 12.05.2015, 20:44.

[26] N. Otsu, A Threshold Selection Method from Gray-Level Histogram, IEEE Transactions on Systems, Man, and Cybernetics 9: 62-66, 1976.

[27] Analiza algoritmilor de segmentare a imaginilor, Universitatea Tehnică a Moldovei, http://www.utm.md/meridian/2010/MI_2_2010/4.Calmicov%20I.%20Analiza%20algoritmilor.pdf, Accesat: 26.11.2015, 23:58.

[28] S.S. Al-amri, N.V. Kalyankar, S.D Khamitkar, A Comparative Study of Removal Noise from Remote Sensing Image, Journal of Computing 2(5):83-86, 2010.

[29] R.A. Fisher, Theory of statistical estimation. Proc. Cambridge Phil. Soc., 22: 700-725, 1925.

[30] D. Csetverikov, Basic Algorithm for Digital Image Analysis-a course, Institute of Informatics, Eotvos Lorand University Budapest, Budapest, 2003.

[31] O.R. Vincent, O. Folorunso, A Descriptive Algorithm for Sobel Image Edge Detection, Proceedings of Informing Science & IT Education Conference 97-107, 2009.

[32] J. Canny, A computational approach to edge detection, IEEE Transactions on Pattern Analysis and Machine Intelligence 8(6):679–698, 1986. doi: 10.1109/TPAMI.1986.4767851

[33] R.C. Gonzalez, R. E. Woods, Digital Image Processing, 2nd ed. Prentice Hall, 2002.

[34] G.T. Shrivakshan, A Comparison of various Edge Detection Techniques used in Image Processing, IJCSI International Journal of Computer Science Issues 9, 5(1), 2012.

[35] M. Barlaud, Wavelets in Image Communication, Elsevier, 1995.

[36] A. Frangi, W. Niessen, K. Vincken, M. Viergever, Multiscale vessel enhancement filtering, Medical Image Computing and Computer-Assisted InterventationMICCAI98 130-137, 1998.
[37] G. Azzopardi, N. Petkov, Automatic detection of vascular bifurcations in segmented retinal images using trainable COSFIRE filters. Pattern Recognition Letters 34:922–933, 2013.
[38] S. Chaudhuri, S. Chatterjee, N. Katz, M. Nelson, Detection of blood vessels in retinal images using two-dimensional matched filters, IEEE Transactions on Medical Imaging 8(3):263-269, 2002.
[39] P. Smets, R. Kennes, The transferable belief model, Artif. Intel. 66(2):191-234, 1994.
[40] L. Moraru, **C.D. Obreja**, Retinal vessel enhancement based on Gaussian function, AIP Conference Proceedings 1796:040007-1, 2017. doi:10.1063/1.4972385.
[41] S. Betrabet, C.K. Bhogayta, Structural Similarity based Image Quality Assessment using full reference method, International Journal of Scientific Engineering and Technology 4(4):252-255, 2015.
[42] S.E. Umbaugh, Digital Image Processing and Analysis: Human and Computer Vision Applications with CVIPtools, Second Edition, CRC Press, 2010
[43] S.S.R. Dhanushkodi, V. Manivannan, Diagnosis system for diabetic retinopathy to prevent vision loss, Applied Medical Informatics 33(3):1–11, 2013.
[44] R.M. Wallingford, E.M. Siwek, J.N. Gray, Application of Two-Dimensional Matched Filters to X-Ray Radiographic Flaw Detection and Enhancement, Review of Progress in Quantitative Nondestructive Evaluation, 879-886, 1992.
[45] N. Otsu, IEEE Trans. Syst. Man. Cybern. 9:62-66, 1979.
[46] W. Enders, Applied Econometric Time Series, First Edition, Edited by John Wiley & Sons, Inc., U.S.A., 269-270, 1995.
[47] T. Mitchell, Machine Learning, McGraw-Hill, New York, 1997.
[48] L. Simar, Applied Multivariate Statistical Analysis, Springer, 2004.
[49] B. le Roux, H. Rouanet, Geometric Data Analysis: From Correspondence Analysis to Structured Data Analysis, Kluwer, Dordrecht, Olanda.
[50] S.M. Lynch, Introduction to Applied Bayesian Statistics and Estimation for Social Scientists, Springer, 2009.
[51] A.K. Jain, R.C. Dubes, Algorithms for Clustering Data, Prentice Hall, Englewood Cliffs, New Jersey, 1988.
[52] A. Hineburg, D.A. Keim, Clustering methods for large databases: From the past to the future. Technical report, ACM SIGMOD Tutorial, 1999.
[53] Algoritmi de grupare, http://cifr.cs.pub.ro/ullman/cluster1-ro.pdf. Accesat: 27.10.2015, 16:33.
[54] J.M. Keller, M.R. Gray, J.A. Givens Jr., A Fuzzy K-Nearest Neighbor Algorithm, IEEE Transactions on Systems, MAN, and Cybernetics, SMC-15(4), 1985.

[55] Morphological Image Processing, https://web.stanford.edu/class/ee368/Handouts/Lectures/2014_Spring/Combined_Slides/7-Morphological-Image-Processing-Combined.pdf. Accesat: 24.08.2016, 19:40.

[56] D.W. Zimmerman, A Note on Interpretation of the Paired-Samples t Test, Journal of Educational and Behavioral Statistics, 22(3):349-360, 1997.

[57] R.D. Nowak, Wavelet-Based Rician Noise Removal for Magnetic Resonance Imaging, IEEE Transactions on Image Processing 8(10):1408-1419, 1999.

[58] IMAGERET, Optimal Detection and Decision-Support Diagnosis of Diabetic Retinopathy, http://www.it.lut.fi/project/imageret/. Accesat: 16.05.2016, 18:20.

[59] H. Leung, J.J. Wang, E. Rochtchina et al, Relationships between age, blood pressure, and retinal vessel diameters in an older population, Invest Ophthalmol Vis Sci. 44:2900–2904, 2003.

[60] Image processing and analysis in Java, National Institutes of Health, http://rsb.info.nih.gov/ij/docs/index.html. Accesat: 12.02.2016, 16:20.

[61] P. Zhu, F. Huang, F. Lin, Q. Li, Y. Yuan, Z. Gao, F. Chen, The Relationship of Retinal Vessel Diameters and Fractal Dimensions with Blood Pressure and Cardiovascular Risk Factors, PLoS One 9(9), 2014.

[62] Whole Brain Atlas (WBA), http://www.med.harvard.edu/aanlib/. Accesat: 09.04.2016,13:30.

[63] A Torrent, A Bardera, A Oliver, J Freixenet, I Boada, M Feixes, R Martí, X. Lladó, J. Pont, E. Pérez, S. Pedraza, J. Martí, Breast density segmentation: a comparison of clustering and region based techniques, Digital Mammography 9-16, 2008.

Research results

Articles published in ISI journals

1. Luminiţa Moraru, **Cristian-Dragoş Obreja**, Simona Moldovanu, Antoaneta Ene, Anjan Biswas, Blood Pressure and Flow Values in Small Vessels Angioarchitectures: Application for Diabetic Retinopathy, Romanian Journal of Physics, vol. 61, no. 7-8, pp.1287-1298, 2016

Book chapter in prestigious publishing houses

1. Luminita Moraru, **Cristian-Dragos Obreja**, Nilanjan Dey, Amira S. Ashour, Dempster-Shafer Fusion for EFFECTIVE Retinal Vessels' Diameter Measurement, chapter in book: Soft Computing In Medical Image Analysis, Elsevier S&T Books, EDS. - Nilanjan Dey, Amira S. Ashour, Fuqian Shi, Valentina E. Balas, No. of pages: 292, Language: English, Published: 30th January 2018, Elsevier, Academic Press, ISBN: 9780128130872, https://www.elsevier.com/books/soft-computing-based-medical-image-analysis/dey/978-0-12-813087-2

Articles published in ISI indexed volumes

1. Simona Moldovanu, **Cristian-Dragoş Obreja**, Luminiţa Moraru, Threshold selection for classification of MR brain images by clustering method, AIP Conference Proceedings, 1694, 040005; doi: 10.1063/1.4937257, 2015.

2. Luminiţa Moraru, **Cristian-Dragoş Obreja**, Simona Moldovanu, Assessment of vessel diameters for MR brain angiography processed images, AIP Conference Proceedings, 1694, 040008; doi: 10.1063/1.4937260, 2015.

3. Luminiţa Moraru, **Cristian-Dragoş Obreja**, Retinal vessel enhancement based on Gaussian function, American Institute of Physics AIP Conf. Proc. 1796, 040007-1–040007-6; doi: 10.1063/1.4972385, 2017.

Articles published in BDI journals

1. Luminiţa Moraru, **Cristian-Dragoş Obreja**, Georgescu E. Monica, Simona Moldovanu, Characterization of Vascular Tree: Responses of Blood Pressure and Flow to Branching Patterns with Various Geometries, Annals Of “Dunarea De Jos” University Of Galati Mathematics, Physics, Theoretical Mechanics, Fascicle II, Year VI (XXXVII) Special Issue, pp. 142-149, 2014.

2. Luminița Moraru, Simona Moldovanu, **Cristian-Dragos Obreja**, A survey over image quality analysis techniques for brain MR images, International Journal of Radiology, vol. 2, no. 1, pp. 29-37, June 2015

3. Luminiţa Moraru, **Cristian-Dragoş Obreja**, Georgescu E. Monica, Assessment of Retinal Vascular System Measurement Methods over Retinal Images from DRIVE Database, Annals Of "Dunarea de Jos" University Of Galati Mathematics, Physics, Theoretical Mechanics, Fascicle II, Year VII (XXXVIII), no. 1, pp. 14-20, 2015.

4. Luminiţa Moraru, **Cristian-Dragoş Obreja**, Vlad Andrei Moraru, Comparative Assessment of Retinal Vasculature using Matched Filtering, Annals Of "Dunarea de Jos" University Of Galati Mathematics, Physics, Theoretical Mechanics, Fascicle II, Year VIII (XXXIX), no. 1, pp 5-12, 2016.

5. Luminița Moraru, **Cristian-Dragoș Obreja**, Emilian Dănilă, The accuracy of retinal vessel diameter measurement based on pixels distribution and fractal representation, Annals Of "Dunarea de Jos" University Of Galati Mathematics, Physics, Theoretical Mechanics, Fascicle II, Year IX (XL), no. 1, pp 18-25, 2017.

Articles communicated at national and international conferences

1. Simona Moldovanu, **Cristian-Dragoş Obreja**, Luminiţa Moraru, Threshold selection for classification of MR brain images by clustering method, Physics Conference TIM-14, 20-22 November 2014, Timișoara, România, http://www.timconference.com/.

2. Luminiţa Moraru, **Cristian-Dragoş Obreja**, Simona Moldovanu, Assessment of vessel diameters for MR brain angiography processed images, Physics Conference TIM-14, 20-22 November 2014, Timișoara, România, http://www.timconference.com/.

3. Luminița Moraru, **Cristian-Dragoș Obreja**, Emilian Dănilă, Evaluarea metodelor de măsurare a diametrului vaselor retiniene pentru diferite afecțiuni, Conferinţa ştiinţifică internaţională a doctoranzilor „Tendinţe contemporane ale dezvoltării ştiinţei: viziuni ale tinerilor cercetători", Academia de Stiinte a Moldovei, 10 martie 2015, Chisinau, Rep Moldova

4. Luminiţa Moraru, **Cristian-Dragoş Obreja**, Georgescu E. Monica, Assessment of Retinal Vascular System Measurement Methods over Retinal Images from DRIVE Database, Scientific Conference of Doctoral Schools from "Dunărea de Jos" University of Galati (CCSD-UDJG 2015), Galaţi, 4-5 June 2015, Section 4. Advanced investigation methods in environment and biohealth

5. **Cristian Obreja**, Simona Moldovanu, Victorita Ştefănescu, Luminita Moraru, "Entropic characterization of random cerebral bio structures in MR images", Scientific Conference of Doctoral Schools from "Dunărea de Jos" University of Galati (CCSD-UDJG 2015), Galaţi, 4-5 June 2015, Section 4. Advanced investigation methods in environment and biohealth

6. Luminiţa Moraru, **Cristian-Dragoş Obreja**, Retinal vessel enhancement based on Gaussian function, Physics Conference TIM 15-16, 26-28 May 2016, Timișoara, România, http://www.timconference.uvt.ro/.

7. Luminiţa Moraru, **Cristian-Dragoş Obreja**, Vlad Andrei Moraru, Comparative Assessment of Retinal Vasculature using Matched Filtering, Scientific Conference of Doctoral Schools from "Dunărea de Jos" University of Galati (CCSD-UDJG 2016), Galaţi, 2-3 June 2016, Section 4. Advanced investigation methods in environment and biohealth.

8. Luminița Moraru, **Cristian-Dragoș Obreja**, Emilian Dănilă, The accuracy of retinal vessel diameter measurement based on pixels distribution and fractal representation, Fifth Scientific Conference of Doctoral Schools from "Dunărea de Jos" University of Galati (CCSD-UDJG 2017), Galati, June 8-9, 2017, Section 4 - Advanced Investigation Methods in Environment and Biohealth.